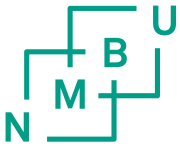
U
B
M
N

List of Figures

List of Tables

Abstract

Deep River AS(Drøbak, Norway) have developed a water current turbine for river, tidal and ocean currents. The turbine is designed to convert the kinetic energy in the water into green renewable electric energy for grid or off-grid systems. The company have signed a contract of interest with the Lithuanian Inland Waterways Authorities. The contract states that if the prototype performs within the expectations there will be a renewed contract with a purchase of 100 turbines. The contract is worth NOK 350 mill.

Before Deep River conducts a prototype test (August 2014) there have previously been performed a series of experiments and simulations to get proof of concept.

This thesis covers the planning, performance and analysis of a small scale experiment, and a computational fluid dynamics (CFD) simulation. In the interest of comparing the experiment with the simulation was the simulated system modelled after the experimental system.

The experiment where performed on the Deep River small scale turbine in a wave tank. The wave tank was installed with equipment for generating continuous flow. There were a number of computer programs used to prepare, run, and process the results of the CDF simulation;

- SolidWorks
- ANSYS Workbench
- ANSYS DesignModeler
- ANSYS Mesh
- ANSYS CFX-pre
- ANSYS CFX
- ANSYS CFX-post

SolidWorks and DesignModeler was used for model preparation. ANSYS Workbench was used to simplify the cooperation between the ANSYS programs. The mesh settings were set and generated in ANSYS Mesh. CFX-pre was the used pre-processor where all the conditions for the system was set. CFX solved the iteration upon the mesh, and the results were graphically processed in CFX-post.

The experimental setup required a contraption that could evenly spread the flow, even when it had to go through an expansion from a 100 mm to a 300 mm diameter pipe and through a 90 degree bend. A pump nozzle was designed and constructed to fill this purpose.

The experiment and simulation was found to have significant differences in their systems, and for that reason was not directly comparable. This made it difficult to draw conclusions from the experiment and CFD simulation.

Contents

1 Introduction

In 2011, nearly 1.3 billion people, or almost one in five of the world's population did not have access to electricity [, IEA(n.d.]. Access to electricity is an invaluable necessity in a welfare state; it provides the foundation for improved healthcare, education, and growth within local communities [Simon Rolland, 2011].

More than 80% of the population without access to electricity live in rural areas [, IEA(n.d.]. In such areas, for example in rural Africa, the electricity produced is commonly provided by diesel gensets [S. Szabó, 2011]. A diesel genset is a diesel motor driving an electric generator, and may produce electricity at the cost of fuel [Simon Rolland, 2011]. The costs that come with purchase, fuel and maintenance of a genset might be affordable considering all the benefits, but unfortunately gensets are also noisy and polluting. The demand for electricity production in rural areas are increasing, and renewable alternatives are continuously being developed to meet these demands [for Rural Electrification, n.d.]. As rural communities tend to assemble near water, such as rivers [M.J. Khan, 2008], technology utilizing the river current as an energy source has proven to be a possible contribution to a clean, long term solution [Sørnes, 2010].

River Current Turbine Technology There are many different concepts developed to convert energy in water currents to electrical energy. These concepts are separated into two categories, depending on the alignment of the rotating axle relative to the water current. The two categories are turbines with axial flow(figure 1), and turbines with cross axial flow(figure 2) [Sørnes, 2010].

The axial turbines have axles oriented parallel to the water current (as seen in figure 1(a) and (b), and have similarities to the technology used for windmills. Figure 1(c) have an inclined axle but is still driven by the forces parallel to the axle.

Figure 1 and 2 gives an overview of different turbine technologies.

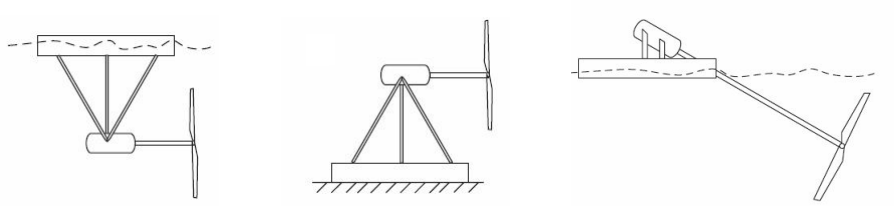

(a) (b) (c)

Figure 1: Axial Flow Turbines: (a) Floating Mooring, (b) Rigid Mooring, (c) Inclined axle.

The cross flow turbines illustrated in figure 2 have a rotational axis orthogonal to the water current. There are two subcategories within cross flow turbines, which are turbines with vertical axis of rotation, or turbines with in-plane axis of rotation. Turbine types with with vertical axis of rotation is illustrated in figure 2(a) to (e). Figure 2(f) is an in-plane axial turbine, often called floating waterwheels. The Deep River turbine is an in-plane cross flow turbine, but this turbine will be fully submerged.

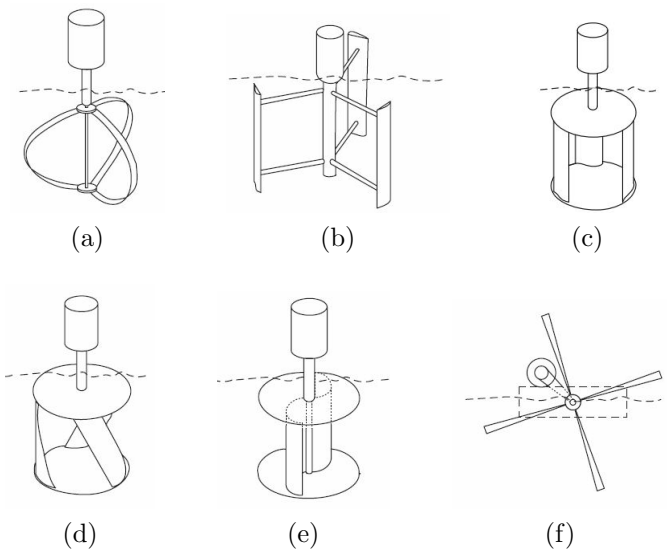

Figure 2: Cross Flow Turbines: (a) Darrieus (b) H-Darrieus, (c) Squirrel Cage Darrieus (d) Helical/Gorlov, (e) Savonius, (f) In-Plane.

Deep River AS Deep River AS was started by Reidar Vestby in 2008 in Drøbak, Norway.

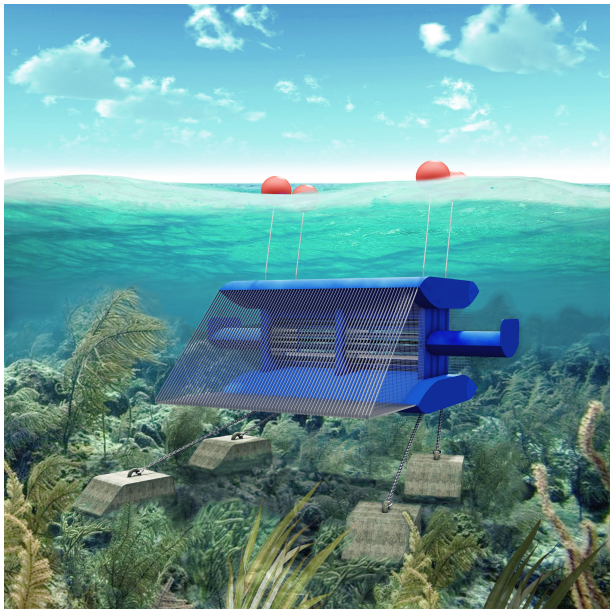

Figure 3: The Deep River Turbine

The Deep River turbine was inspired by the waterwheel, a concept which have served humans well for over a thousand years [Vestby, 2014, M.J. Khan, 2008]. Through innovation, Vestby has been working to create a concept that effectively harvests the energy from river-, ocean-, and tidal currents. The result is an in-plane cross flow turbine, designed to convert kinetic energy in the water current to mechanical energy, and ultimately electrical energy.

On the design and construction phase of developing new technology there are several problems and challenges that must be considered. Some of the problems and challenges for water current turbines (WCT) are listed below [Vestby, 2014].

- Mooring system
- Placement in river/ocean.
- Self starting
- Corrosion
- Fouling
- Hydraulic leakage
- Debris
- Fish and marine animals
- Ice
- Floods
- Boats
- Environmental impact

Potential investors and buyers are interested in all the points above, but questions regarding maintenance, life time expectancy, and price/kWh, are also highly relevant.

Deep River AS have signed a contract of intent with Lithuanian Inland Waterways Authority which states that if the prototype performs within the predefined frames there will be a purchase of a hundred turbines over the following three years. This contract, if all the expectations are fulfilled, have a value of 350 million NOK [NORWEA, 2013, Vestby, 2014].

In the process of developing new technology, experiments are important to control that the technology, or the technology until that stage, performs as expected. A series of small experiments might be less expensive than a full scale test, and will still provide some credibility to the technology. For technologies based on fluid flow, there are several computer programs (ANSYS CFX, Comsol Multiphysics, Solid Works Flow Simulation, e.g.) that are able to simulate the physics of moving water around or through a model.
Some of the tests that might be performed on a WCT are listed below:

- Computer simulation of the essential part (E.g. a turbine blade)
- Computer simulation of the whole model
- Test of essential part in tank
- Small Scale Experiment in tank
- Small scale on-site
- Full Scale on-site (prototype)

Before the scheduled prototype testing of the Deep River turbine at the end of August 2014, the company has performed a series of experiments and simulations. This thesis covers an experiment and simulation performed on a simplified small scale version of the Deep River turbine. In order to compare the two methods and their results, the turbine and the

physical conditions in the small scale experiment were tried adopted in the CFD simulation. Important factors regarding the simulation and experimental testing are accounted for and explained.

2 Theory

2.1 A Closed Circuit System

A closed circuit system utilizes a series of pipes and bends to keep a relative small amount of water constantly flowing. Each pipe and bend influences the water flow in different ways.

Each pipe and bend will contribute with a pressure loss in the pipe system [J. F. Douglas, 2005], and some pressure will be lost due to leakage. Most of the leakage is expected to be at the nozzle area, where there are several parts fitted together. The total pressure loss reduces the maximum flow rate that can be driven through the pump.

The velocity profile inside the pipes are affected by the bends. An example of how the velocity profile may be affected can be seen in figure 4. The profile in a straight pipe is dependent on the wall roughness, fluid viscosity, the diameter of the pipe and the velocity of the flow [J. F. Douglas, 2005]. The level of turbulence in a circular pipe is decided by the Reynolds number, which is given by equation 1 below.

$$Re = \frac{\rho \, \overline{V} \, D}{\mu} \tag{1}$$

In equation 1 Re is Reynolds number, ρ is the density of the fluid, $\overline{V}$ is the average velocity in the pipe, D is the characteristic length and μ is the viscosity of the fluid. For a circular pipe the characteristic length corresponds to the diameter of the pipe.

The bends close to the inlet or outlet will affect the flow velocity gradients that enters the pool.

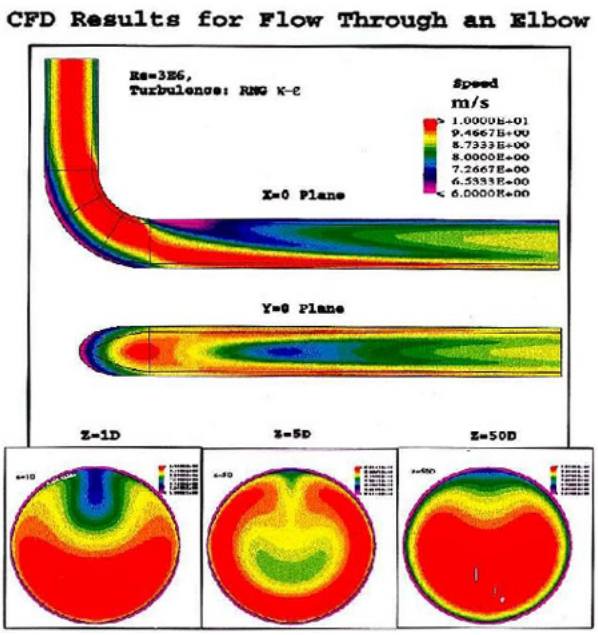

Figure 4: CFD Simulation of Fluid Flow through an Elbow Bend. Picture Courtesy of JDF & Associates, [Furness, 2007]

2.2 Biofouling

Biofouling may affect the efficiency of marine current turbines (MCT). J. A. C. Orme [2001] covers this effect, and mentions three types of biofouling; animals, weed and slime. J. A. C. Orme [2001] concludes that low levels of fouling could cause 20% reduction in efficiency, while higher levels of fouling could cause a reduction of 70%. The presented numbers are from tests on a stationary blade, and cannot directly predict the effect on a turbine with moving blades.

2.3 CFD - Computational Fluid Dynamics

The study of physics is about trying to understand how the world really works. After observing natural occurrences, scientists have proposed mathematical equations that model that behaviour[H. K. Versteeg, 1995]. These models are often simple per ce, but the modeling of large systems (or the interaction between different systems) often require time consuming iteration. By feeding the mathematical models into a computer the iterating process is made much faster, and the computer does not do miscalculations.

To be able to create a simulation it is necessary to provide the computer program with some vital information about the system [H. K. Versteeg, 1995]. Information such as what equations to use, what boundary conditions there are, and to what accuracy the solver should work to achieve [ANSYS Inc, b].

2.4 SolidWorks (SW)

SolidWorks(2014) is 3D engineering program with which one can design models, do stress-analysis or flow simulations (using the add-in called 'SolidWorks Flow Simulation') e.g.

2.5 ANSYS Workbench

Ansys Workbench (R14.0) is a user friendly drag-and-pull program which makes it easy to structure the cooperation of the different ANSYS programs. All the ANSYS programs can be run separately without Workbench, but Workbench simplifies the experience and provides an automatic filing system that order all the file types used in a session.

2.6 DesignModeler (DM)

ANSYS DesignModeler (R14.0) is a 3D modelling program for designing models and for model preparations. DM has features similar to SolidWorks, but the user interface is different and not as user friendly.

The features below were used in preparing the model.

2.6.1 Multi-Body-Parts

Multi-Body-Part is best described by first defining a body. One body is a piece of something, like the seat on a bicycle, that can be combined with other bodies (wheels, frame, steering etc.) to create e.g. a bicycle. Multiple bodies may be connected, but will be treated as separate bodies that are connected [ANSYS Inc, c]. Multiple bodies that are defined together as a 'Multi-Body-Part' will be treated as if they together formed only one body, or in other words: they share topology. This becomes apparent during the meshing process, since multi-body-parts will have a conformal mesh, while multiple bodies together may have a non-conformal mesh (see section 2.7.5).

2.6.2 Enclosure

Enclosure is a feature that creates a fluid volume that encases one or more selected volumes [ANSYS Inc, c]. Already existing geometry can also be converted to an enclosure fluid. This feature is used to model the fluid domain (all areas where there will be fluids). All selected parts will be excluded from the enclosure-part. In cases where only flow simulation is of interest, it is possible to 'suppress' all solid parts and just have the fluid-domain. This may in some cases reduce the mesh-size considerably and thereby also the time it takes to mesh and solve. Note that the solid parts is necessary if heat-transfer is of interest. The geometry that is to be encased must be fully within the enclosure-volume; which means that the distance from the enclosure walls to any of the components that are enclosed must be larger than zero.

2.6.3 Slice

The slice feature can split up parts by different methods [ANSYS Inc, c]. This is useful if one wants to select different areas of a domain to have different mesh settings. A non-sweepable body (see section 2.7.2) may become sweepable by splitting a part with the slice feature.

2.6.4 Domains

Domains are separated from each other by the different settings that applies to the domains [ANSYS Inc, b]. The fluid volume is mostly in one stationary domain (here called the Fluid Domain), but there is also an area that is rotating. To define an area as rotating it must be encased in a defining geometry [Holst, 2014]. In the case of this thesis the defining geometry was a cylinder, called rotational domain, that encased the turbine blades and the anchoring discs. This cylinder was first created as an enclosure around the blades (see enclosure above), then later used to define the rotational domain.

2.6.5 Symmetry

The symmetry feature is located in DesignModeler, and as the name suggests, may simplify a simulation by defining one or more symmetry planes [ANSYS Inc, c]. A symmetry plane is a plane where the model is symmetrical on both sides, and a model may have more than one symmetry plane. Using the symmetry feature may shorten the simulation time, but one also defines the results of the simulation to be symmetrical. In cases with great turbulence there may be symmetrical models but asymmetrical results. These asymmetrical results are lost in favour for symmetrical (incorrect) results if one uses the symmetry feature [Holst, 2014].

2.7 Mesh

When creating the mesh it is essential to capture all the important areas in fine mesh, but for large models it is also important to let the less important areas have a rougher mesh. If the mesh consists of a large amount of elements, the mesh will take a lot of time to generate, and the solver will use a lot of time iterating upon the mesh. How fine the fine mesh needs to be, and how rough the rough mesh can be, is determined by the point when the results no longer are mesh dependent [Holst, 2014]; see below.

2.7.1 Mesh Dependent Results

Mesh dependent results are highly unwanted. The generated mesh is insufficient to capture all the physical elements in the simulation, and therefore the results changes if one increases or decreases the mesh resolution. Mesh independent results are achieved when the changes in the results are insignificant even when the mesh resolution is increased [Holst, 2014].

To determine if a mesh is truly good, one must go through the process of adjusting the resolution and look at the results. If there are relevant changes in the results, the mesh should be improved. For big models that demand a lot of a computer capacity, this is a tedious process.

2.7.2 Mesh Methods

Note that there are six methods available for 3D geometries: Tetrahedral, Sweep, MultiZone, Hex Dominant, CutCell, Automatic and Interoperability between the different meshing methods. The following paragraphs will give a short description of the two methods used in this thesis and their specialities. For more information on the different kinds, see ANSYS Inc [a].

Tetrahedral and Hexahedral Tetrahedral mesh cells are highly automatic in generation [ANSYS Inc, a, Lecture 3.]. This means that selecting tet-mesh most often succeeds and gives a working mesh. On the negative side tet-mesh requires more memory and calculation time per node than hex-mesh and it works badly in environments with high shear stress.

Hexahedral mesh cells is the best element with regards to memory and calculation timer per element [ANSYS Inc, a, Lecture 3.]. Hex-mesh is the best shear layer element, and is recommended by ANSYS to always be used as such in the form of inflation layers (see section 2.7.7) on all wall boundaries affecting the simulation. The fault of hex-mesh lies in its degree of automation. It may work well for very simple geometries, but will fail before tet-mesh when the model gets complicated.

Sweep The sweep feature is a fast way of generating either prisms or hexahedral mesh cells [ANSYS Inc, a, Lecture 3.]. This feature generates the surface mesh on a source surface first, and sweeps it towards a target surface, placing mesh elements that are evenly distributed. It is necessary that the source and target surfaces are connected by a smooth volume.

Automatic Mesh This method is robust by using tetrahedral mesh cells, and relatively fast since it will utilize the sweep method where possible [ANSYS Inc, a].

2.7.3 Rotating Mesh

The rotational domain will be set to rotate at a given angular velocity, and the mesh in that domain must follow the rotational movement. By doing this, the topology of the mesh does not need to be updated as it remains the same [ANSYS Inc, b, Lecture 9].

2.7.4 Preparations for Boundary Conditions

In a simulation there may be boundaries that have a greater effect on the results than others. By recognizing to what degree a boundary will affect the simulation, one may adjust the mesh resolution thereafter.

Walls Walls should be covered with inflation layers (see section 2.7.7). Wall boundaries are the main source of vorticity and turbulence. To ensure that the inflation layers are thin enough to capture the physics close to the walls, there are criteria for the Y^+ parameter (see section 2.7.8).

Inlet/Outlet The boundary conditions at the inlet and the outlet will in most cases affect the whole system. If precise values for the inlet and outlet conditions are used, it is recommended to use a fine mesh in the vicinity of the boundary surfaces to maintain that precision [Holst, 2014].

2.7.5 Conformal vs. non-Conformal Mesh

By creating multi-body-parts, one also selects that the mesh needs to be conformal across the borders of these parts. A conformal mesh means that the mesh nodes on the contact region of the bodies will be lined up and connected [ANSYS Inc, a]. In contrast non-conformal mesh will not automatically be lined up and connected on a contact region. A non-conformal mesh will reduce the credibility of the mesh since the residuals will be larger in the contact region than with a conformal mesh.

2.7.6 Mesh Sizing

By creating a mesh sizing on a surface or body, one selects that that surface or body is important, and that the surface or body needs finer mesh. By e.g. adjusting the element size on a surface, one may indicate how small the mesh elements should be [ANSYS Inc, a].

2.7.7 Inflation Layer

Inflation extrudes the mesh on a surface along the normal of the surface [ANSYS Inc, a]. This causes the inflated cells to be like slices, an inflated layer, of the inflated mesh (tetmesh or hexmesh). This is done where there are expected high gradients normal to the surface but small changes perpendicular to the surface. The high gradients normal to the surface will then be captured by the fine inflated mesh, while the small gradients perpendicular to the surface will be treated as normal.

In some cases it is necessary to apply a mesh sizing to get a finer mesh resolution before placing the inflation mesh on a surface [Holst, 2014]. The first layer thickness (FLT) and number of layers (N) are two of the adjustable settings. Whether an inflation layer is thin enough that the physics can be captured, can be checked in CFD-post by looking at the Y^+ parameter on the surfaces.

2.7.8 Y^+

Y^+ is a dimensionless parameter used to determine if the first wall node is in the laminar or logarithmic section from the wall [ANSYS Inc, b, Lecture 7.]. The Y^+ parameter is among other factors dependent on the flow velocity along a surface, and the distance (Y) from the surface to the first mesh node. Y^+ values between 10 and 15 places the node in a transitional area between laminar and logarithmic behaviour of the boundary layer, which should be avoided. The desired Y^+ value is dependent on whether one uses a logarithmic-based wall function or a near-wall resolving approach. Logarithmic-based functions should have an $Y^+ \approx 30 - 300$, while the near-wall resolving approach should have an $Y^+ \approx 1$.

2.7.9 Defeaturing Length

During the mesh generation all the lines, gaps, and angles are processed. Depending on the relevance set for the mesh, there is set a defeaturing length. All the gaps and lines that are shorter/smaller than the defeaturing length will be neglected by the mesh generator [ANSYS Inc, a]. For geometries with small important pieces, the defeaturing length must be shorter than the length of the surfaces belonging to the smallest important piece.

2.8 ANSYS CFX-pre

In CFX-pre it is determined which physical aspects are relevant for the simulation, the boundary conditions are also placed and given a value, and the criteria for the simulation and solving the system are set [ANSYS Inc, b]. Basically, CFX-pre prepares the equations with constants and variables, and sets solver criteria. This is done so that the solver (ANSYS CFX) may use the data from CFX-pre, and solve those equations upon the mesh provided by ANSYS Mesh.

CFX-pre provides two options for the analysis type. Both options and some derivatives are explained below.

2.8.1 Steady State Simulation

A steady state simulation is a false-transient simulation, and not suited to solve time dependent simulations [ANSYS Inc, b, Lecture 5.]. When running a simulation with the steady state condition, the computer starts iterating with a set of initial conditions at $t = 0$, and each following time step gets iterated once. In the start phase the flow from the pump outlet travels in the domain, causing previously stationary water to move. The solver works on quantifying these changes, but it is unlikely that it will find a converged solution with the single iteration the steady state simulation gives for each time step [ANSYS Inc, b, Lecture 5.].

When the fluid that exited the pump outlet enters the pump inlet, the start phase ends [Holst, 2014]. After that point the system should start to stabilize. How stable the system becomes is dependent on the transient variables, which will change the flows to some degree each time step. If the changes are oscillating, the steady state simulation might not be able to converge. A solution is satisfactory convergent in most cases when it reaches the convergence point, see section 2.9.

Even though the steady state simulation might be unable to converge, and the results may be questionable, there are certain benefits of running it. By running a steady state simulation before the transient simulation one may use the solution from the first as the initial conditions on the second [Holst, 2014]. This puts the transient simulation in a better starting position. A steady state simulation is faster than the transient simulation, and therefore it may be wise to utilize the steady state simulation in the start phase. The transient simulation takes over for the steady state simulation when the flow have developed and is relatively stable. The transient analysis should then work to get the simulation to converge at every time step [Holst, 2014].

2.8.2 Transient Simulation

Time dependent systems are simulated by using a transient analysis method [ANSYS Inc, b, Lecture 11.]. This method recognizes that the changes between two time steps may be bigger than what can be solved with one iteration, and gives the opportunity to set a minimum and maximum number of iteration steps that can be taken for each time step. After the solution has been found for e.g. the tenth time step, transient effects may change the flow. The solver may be able to find a converged solution within the given amount of iterations, or it may not. If it fails, that time step will have an inaccurate, non-convergent solution.

If the solver is able to find a converged solution for a time step before it reaches the maximum number of iterations, it jumps to the next time step.

2.8.3 CFX-pre Settings

There are many different settings in CFX-pre, and not all are easily explained. This thesis will not cover all the different settings for steady-state or transient simulation, but the more prominent settings is covered below. The actively used settings are presented in the list in section 4.2.5. It is recommended to check ANSYS' "Introduction to ANSYS CFX" (2011) for an in-depth presentation of all the settings.

Rotation The demanded computer resource for using the transient rotor-stator may be large, but is the best for transient simulations where the rotational motion is important [ANSYS Inc, b]. The transient rotor-stator rotational model should not be used in a steady-state simulation since it is inherently unsteady.

Time Step and Transient Results In both steady state and transient simulation the time step must be defined. The time step is essentially how much time there should be between each point in time that should be simulated [ANSYS Inc, b]. If the time step is relatively big, the system may have changed so much that the solver is unable to find the converged solution. If the time step is relatively small, the solver may find the solution, but a simulated time period[1] will need more time points and then also use more real time[2].

Since transient simulations is used to simulate time dependent systems, there is not one result that represents the whole system, but rather one result per time step. The results may be similar, they may be different, but they all corresponds to a specific point in the simulated time [ANSYS Inc, b].

Turbulence Model Turbulence is a relatively large subject within CFD simulations. There are a number of different models with each their strengths and weaknesses. None of the turbulence models have been completely deduced from fundamental principles; all models contain some empiricism [ANSYS Inc, b].

The Shear Stress Transport (SST) model is a hybrid two-equation model that have combined the advantage of two already recognized models; the $k-\epsilon$ and $k-\omega$ models. $k-\epsilon$ have

[1] Simulated time is the accumulation of time steps, and the time period that is simulated in the system.
[2] Real time is the physical time.

its strengths in the freestream area, while $k - \omega$ is a superior model for solving boundary conditions.

After having decided the turbulence model it is necessary to consider what Y^+ values there are on the surfaces. The SST model needs $Y^+ < 300$, or the logarithmic-based wall function will not be valid [ANSYS Inc, b, Lecture 7.]. To take advantage of the $k - \epsilon$ models strengths at low Re (see eq. 1), then $Y^+ < 2$.

2.9 ANSYS CFX

ANSYS CFX (version 14.5.7) is the solver that uses the equations given by CFX-pre to try and calculate solutions as accurately as possible until the point of convergence.

Convergence Convergence is when the residuals from the equations used in the solver have reached, or are lower, than the pre-set convergence point. The convergence point, or the residual target, are for most cases sufficiently low with a value of 10^{-4} [Holst, 2014].

2.10 ANSYS CFX-Post

CFX-post (version R 14.5) handles all the data in the result file from the solver and have different features for presenting the results. The features used in this thesis are relatively self-descriptive and are utilized in section 4.4.

3 Materials

The small scale experiment was performed in a wave tank at Elvebakken Videregående Skole, a high school located in Oslo. A pump and pipe system was installed in the tank to create a closed water flow circuit (see 'Closed Circuit System' in section 2.1).

3.1 Instruments

As the initial measuring instrument for flow velocity in the wave tank proved insufficient, it was replaced by a second instrument. In the following paragraphs the initial instrument is referred to as instrument A, and the second as instrument B.

Instrument A Instrument A is designed to measure the velocity a boat travels relative to the water. The instrument is a product of NASA Marine Instruments, a 'Target 2' speed and distance log. On the web page of NASA Marine Instruments the technical specifications for the log computer and paddle wheel is given. The relevant technical information for this thesis is that the speed range is from 0 to 30 knots with 0.1 knot increments, and that it utilizes a proven paddle wheel sensor. This gives that the lowest increment the sensor can distinguish is 0.05 m/s.

An image of the NASA Marine Log Computer is shown in figure 5a, and figure 5b shows the paddle wheel sensor.

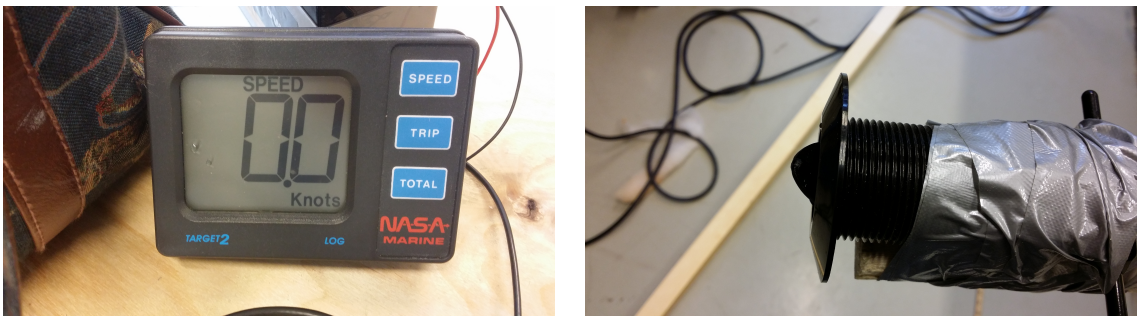

(a) NASA Marine Log Computer. (b) Paddle Wheel Sensor.

Figure 5: Flow Velocity Measuring Instrument A

Instrument B Instrument B (MiniController MC20 with a MiniWater®20 Mini probe, Schiltknecht Messtechnik AG, Switzerland) have a range from $0.03m/s$ to $10m/s$, and an increment of $0.01m/s$. The accuracy of the instrument is given below.

$$accuracy = \pm 2.0\%\ fs \pm 3.5\%\ rdg \tag{2}$$

The *fs* and *rdg* terms in equation 2 represent the 'full scale' value and 'reading' value respectively. The full scale corresponds to the maximum range of the probe, which is $10m/s$, and the first part of equation 2 then becomes $0.2m/s$.

An image of instrument B is shown in figure 6. The sensor is taped to a lengthening pole, and the face of the sensor was adjusted to be normal to the pole.

Figure 6: Instrument B. The MiniController MC20 and MiniWater®20 Mini.

Both instruments were taped to a wooden pole to lengthen the reach of the equipment and provide means of fastening the instrument in one position, as can be seen in figure 7a, 7b and top of figure 6.

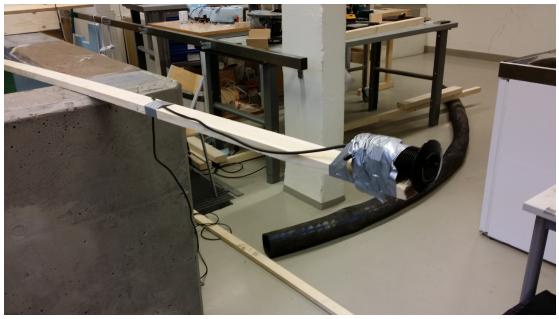

(a) Instrument A Taped to a Pole.

(b) Instrument A Taped to a Pole and Fastened to the Platform.

Figure 7: Using a Lengthening Pole and Fastening to the Platform

3.2 Computer Programs

The computer programs used in this thesis are listed below. For further insight see their respective theory sections.

- SolidWorks (2014)
- ANSYS Workbench R14.0
- ANSYS DesignModeler R14.0
- ANSYS Mesh R14.0
- ANSYS CFX-pre
- ANSYS CFX
- ANSYS CFX-post

3.3 Experiment

Pool Dimensions Figure 8 gives a two dimensional section view of the experimental setup. The dimensions of the pool can be seen in table 1. Table 2 gives the coordinates of the different components centers. Origo and the orientation of the x, y and z- axis is defined in figure 13 on page 28.

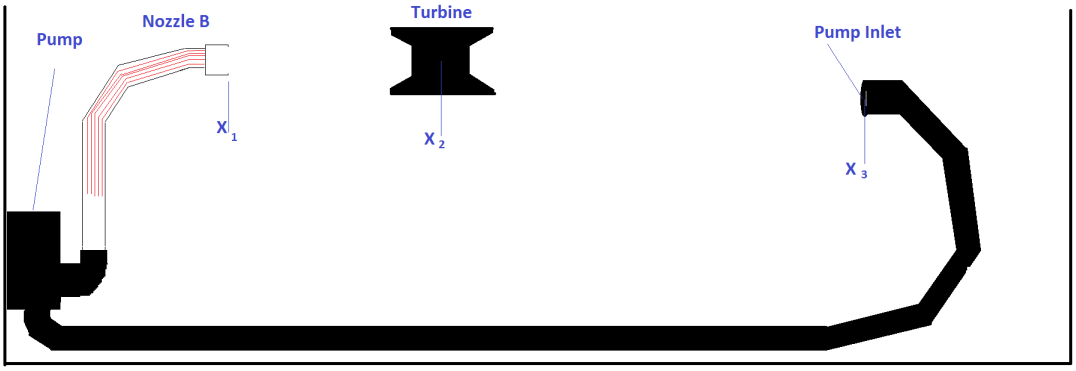

Figure 8: Experimental Setup B.

Table 1: Pool Dimensions.

Length	X	632 cm
Width	Y	224 cm
Depth	Z	223 cm

Table 2: Coordinates of the Components. The Length Coordinate X_N, corresponds to the positions in figure 8.

Center of Component	Position	
Nozzle B/Pump Outlet	X_1	113 cm
	Y_1	112 cm
	Z_1	-19,5 cm
Center of turbine	X_2	263 cm
	Y_2	112 cm
	Z_2	-19,5 cm
Pump Inlet	X_3	437,5 cm
	Y_3	116 cm
	Z_3	-37,5 cm

Shape and Dimensions of Components in Experiment B

Nozzle B The nozzle have a complex construction as shown in the figures on page 40, but the overall shape of the nozzle outlet is that of an ellipse with radius of 14 cm vertically (b = 14 cm) and 15 cm horizontally (a = 15 cm).

Turbine The turbine consists of mainly six different pieces.

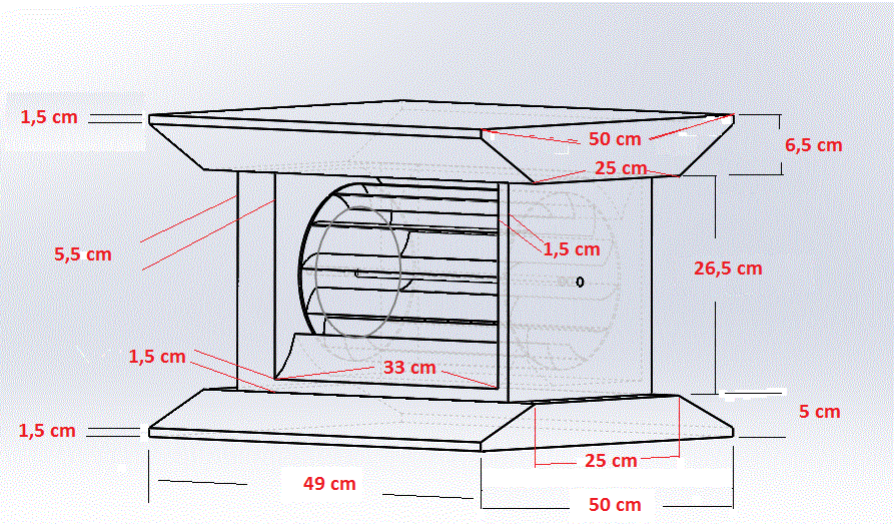

Figure 9: A Wireframe Screenshot of the Turbine with Dimensions. N.B. This figure is upside down and viewed from behind.

The dimensions of the buoyancy platoons and the container is given in figure 9. Note that the platoon on top (should be on bottom) is larger than the other one.

The spoilers have the same dimensions. The blade tips on both span 4.8 cm over the container floor/roof. The tips extend 3.1 cm into the container. The outer curve lengths are 5.7 cm, and the inner lengths are 8.0 cm. The distance from tip to base of the spoilers are 5.5 cm and 7.7 cm on the short and long side respectively.
The blades are made of thin sheet metal, estimated to be 1 mm thick. The length along the curve of the blade are 3.7 cm, while the length from end to end are 3.2 cm. From point to point the blades span 30.0 cm. The front tip is on the edge of the anchoring discs, while the back end are 2.5 cm from the edge at the closest.
The axle is 0.7 cm in diameter.
The anchoring discs locks the position and orientation of the blades, and connects them to the axle. They are 0.3 cm thick, and have a diameter of 20.5 cm.

3.4 Other Equipment

Two different types of work platforms were used as seen in figure 7b and 29c. Both were used with a wooden pole (called a rig) that was rigged to the platform and marked with lines. The lines indicated the horizontal position of the sensor relative to the center of the turbine. The sensor was attached to the lengthening pole, which again was fastened to the rig. The lengthening pole had lines that indicated the depth of the sensor relative to the vertical center of the turbine.

A bubble level was used on the lengthening pole to keep it level and ensure the correct positioning of the sensor (see figure 29b).

4 Method

For this thesis it was planned to do one practical experiment and one computer simulation. The interested party, Deep River AS, would set up everything around the practical experiment so that the experiment could be started in early March. Before the start of the experiment, there were four points on the to-do list;

1. Plan the experimental setup
2. Plan the measuring process
3. Finish a preliminary simulation of the experimental setup
4. Work on the main simulation and be close to finished

4.1 Experimental Setup A

The Deep River turbine is planned to be tested in the river Nemunas (Lithuania), at a site where the river is both wide (over 100 m) and relatively deep (3-4 m). In such a wide river, the turbine will experience very small horizontal velocity gradients. The river is however too shallow to completely eliminate the vertical velocity gradients. For the small experiment to have the most integrity, the velocity parameters into the turbine should be closely matched to the river conditions. In this regard there were four considerations that needed to be accounted for:

1. Some distance between the turbine, pump outlet and pump inlet.

Reason: So that the velocity gradients and turbulence from the pump inlet and outlet would not enter directly into the turbine, but even out over the distance.

2. The surface dimensions of the pump outlet should be larger than the surface of turbine.

Reason: The edges of the flow from the pump outlet will interact with the water in the pool. The interaction of the pump outlet flow with the pool water will, caused by the water viscosity, start movements in the pool water and steal energy from the edges of the pump generated flow (One could argue that all the flow in a pool is pump generated). This gives the foundation of a flow with developing velocity gradients dependent on the distance from the pump outlet.

3. Small velocity gradients across the pump outlet.

Reason: If the velocity gradients across the pump outlet could be made quite small, the required distance between the pump outlet and the turbine could be shorter.

4. Flow from pump outlet directed evenly vertically in regards to the turbine.

Reason: If the flow facing the turbine is not distributed evenly along the vertical axis, the turbine could be given a larger or smaller amount of torque than under river conditions.

4.1.1 Determining the Experimental Setup

A 3D model was created from the measurements of the pool at Elvabakken VGS in Oslo. The actual setup of the experiment was discussed several times, where the main problem was the small size of the pool. The goal was to have a setup that would provide an even distribution of the flow across the cross-section of the turbine and prevent the flow behind the turbine from being overly affected by the pump inlet. The placement of the turbine was determined by an educated estimation by the following criteria:

1. The turbine needed to be as far away from the outlet of the pump as possible to let the flow even out before it entered the turbine.

2. The turbine needed to be far enough away from the pump inlet in order to prevent the suction from the inlet from determining all the flow characteristics behind the turbine.

The turbine was therefore placed 2/3 of the distance between the inlet and outlet towards the inlet. All of the components centers were placed on the center-axis down the length of the pool. The turbine were placed on the bottom of the pool. Since the water depth was uncertain, it was set to be one metre above the top of the turbine for the preliminary simulation. The inlet and outlet to the pump were modelled as two circular discs with a diameter of 0.5 m, and placed on either side of the pool, 0.5 m from the end wall. Inlet/outlet discs were placed with their centers at the height of the center of the turbine to get equal amounts of flow on both sides of the turbine axis.

Setup Description The pool dimensions can be seen in table 3.3 in page 18.

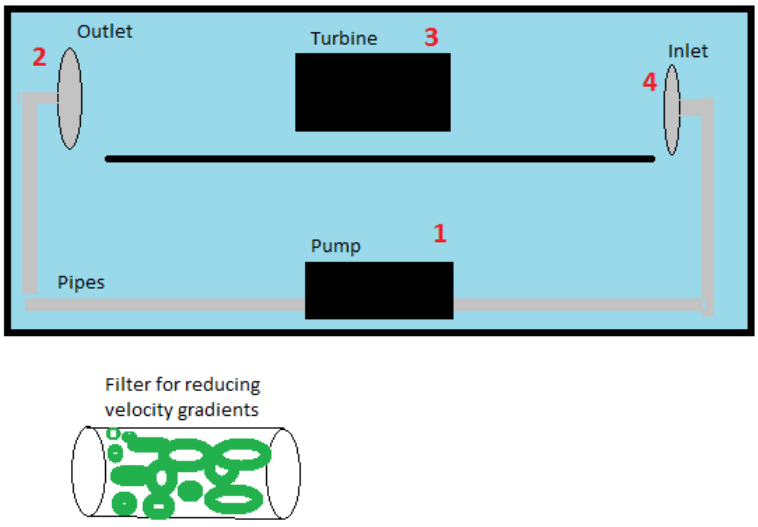

Figure 10: Sketch of the Experimental Setup A: (1) Pump, (2) Pump Oulet (3) Turbine (4) Pump Inlet

Note that the labels 'Outlet' and 'Inlet' on figure 10 corresponds to the pump outlet and inlet, and the flow therefore travels from the pump and into the pipes on the left on

the figure. The bottom part of the figure is an early sketch of a filter for reducing velocity gradients (pipe containing round objects to distribute the flow).
The pump inlet and outlet was placed with a distance of 0.50 m from each end of the pool end walls. Both the inlet and outlet had a diameter of 0.50 m. The inlet and outlet were placed at a depth which centered them according to the turbine. The black line stretching from the bottom of the inlet to the bottom of the outlet is a platform that would hinder the flow from spreading down to the pump.
The container and turbines were placed so that the center were relative to the distance between the inlet and outlet, 1/3 from the pump outlet and 2/3 from the pump inlet.

4.1.2 Preliminary Work with the Model and the Experimental Setup

Deep River AS possessed a 3D model of their turbine which was made in Autocad. This model was exported from Autocad as different file types, but none of the file types were fully compatible with SolidWorks(2014) (SW) or ANSYS DesignModeler. The author had previous experience with SW and its simple user interface, and that is why the model preparations of the Deep River turbine was done in SW instead of ANSYS DesignModeler.

Model Preparation in SolidWorks (SW) The file type that gave the best results when imported into SW was the .igs file. The imported parts were then only recognized as 2D surfaces that coincided, and not recognized as 3D parts (Volumes). A SW feature called 'SolidWorks feature recognition' recognizes the geometry, and sets up a tree of steps that would create the same geometry. This tree of steps is then used to recreate the geometry but now in a fully compatible SW file format. This process was completed for each individual part since 'feature recognition' does not work on very complex geometries with many intersecting surfaces. The separate parts needed to be assembled, but the positioning of the blades demanded more fine tuning than the rest of model. The turbine was therefore assembled first, with only the blades, axle, and supporting construction. Even though the .igs file failed to import smoothly into SW, it was possible to measure the position of each part from that model. This was important in regards to the angles of the blades and their distance from the axle. The container and the two parts designed for buoyancy was assembled in a separate SW assembly. Lastly the turbine assembly was inserted into the container assembly, and these two mated together.

Two cylinders that encased the turbines were created in SW in preparation for the enclosure feature, see section 2.6.2 and section 4.1.3.

Model Simplification in Solid Works Model simplifications are all about removing or remodelling geometrical structures that are demanding more than its fair share of mesh cells. Furthermore, the purpose of model simplification is to reduce the number of mesh cells without reducing the credibility of the mesh and analysis.

The original container had ruffled walls that where straightened out. The stabilizers were discarded to simplify the model. The buoyancy platoons had a separate end point on both

the top and bottom one. These were made separately and poorly, which prevented the surfaces from connecting properly, leaving wedges with small angles. To simplify the geometry the two parts of the buoyancy platoon were remade into one. This change caused the rotational ability of the front end point to be removed, but the surface was made even without small angles. The buoyancy platoons have indents in them that the container is fitted into. These where not sized properly, which made a narrow gap along the container on the top and bottom. The narrow gaps were removed by resizing the indent on the buoyancy platoons.

It was found in ANSYS DesignModeler that the bottom buoyancy platoon and the bottom of the platform created a sharp angle that would demand unwanted large amounts of small mesh elements in the vertex unless it was removed. This was handled by redesigning the platoon so that it came faster in connection with the floor, and thereby widened the angle.

4.1.3 ANSYS DesignModeler

There were a couple of reasons as to why ANSYS was used for the main simulation instead of SW. Firstly, SW has only one mesh-cell-geometry, which is cubes. This makes SW less flexible than ANSYS. Secondly, previous experience with SW has shown that it does not handle rotational domains properly. Ansys CFX is said to handle rotational domains quite well. [Holst, 2014]

Import of CAD and problems with geometry After having designed the experimental setup in SolidWorks, the CAD file was imported into ANSYS DesignModeler while working in the interface of ANSYS Workbench. ANSYS DesignModeler have a repair feature that locates and proposes quick-fixes to problems automatically. This repair feature gives the opportunity to check for e.g. 'Hard Edges' and 'Sharp Angles'. Both of these can give problems during meshing, and it was found that these two were posing a problem for the model.

The problem of 'Sharp Angles' originated at the vertex where the bottom buoyancy platoon connected with the platform. The sharp angle would demand a great amount of small mesh elements in an area that would likely not be important [Holst, 2014], see section 4.1.2 for how this was handled.

The problem 'Hard Edges' originated from misalignments in the geometry and was probably caused during the export/import of the CAD-model. There were several cases of 'Hard Edges', and many of these were small gaps which should not have been there. These were mostly gaps with lengths close to 10^{-6} or smaller. The geometry problems under the category 'Hard Edges' were surpassed by using the 'Virtual Topology' feature along with closely monitoring of the 'Defeaturing length', both of these in Ansys Meshing (see section 2.7).

Multi-Body-Parts Creating a multi-body-part is simple but important. By selecting the parts that are in the setup and creating a multi-body-part of these; one also determines that the mesh needs to be conformal on the borders of these parts (see section 2.7.5).

Enclosure As mentioned in section 4.1.2 there were already two prepared volumes that enclosed the turbines, and these were selected to be used as enclosure volumes. The enclosure feature then automatically creates a fluid body that can be meshed. The solid bodies of the turbines were then suppressed. A second enclosure was made to enclose the inlet, outlet, container and the fluid body that enclosed the turbines. After the second enclosure was made, all the rest of the solid bodies were suppressed, leaving only the two fluid bodies that together encompassed the whole setup.

Slice The pool, and therefore also the area that needed to be meshed, was relatively large for a CFD simulation. One of the steps that were taken as an attempt to reduce the number of mesh elements was to isolate the top of the pool as a separate domain with hexagonal mesh. To create this separate domain, the slice feature needed to know which plane it needed to slice, and an origin point on that plane. An offset of 0.5 m from the top of the turbine was used as the origin point height, the other coordinates were irrelevant. The plane that would be sliced were the plane parallel to the floor. When these input parameters were given, and the slice was generated, there was a new body that needed to be included in the multi-body-part. The new body could then get individual mesh settings.

Symmetry As a way to reduce the mesh generation time and solver time, the symmetry feature was used. The model was symmetrical along the length of the pool. As mentioned in section 2.6.5 non-symmetrical results would not be captured by using the symmetry feature.

4.1.4 Mesh

The creation of the mesh took a long time and was subject to a lot of trial and error. As one can see in the theory part in section 2.7, there are many options for how to create a good mesh, and there may be more than one alternative that gives a good result.

Local Mesh Settings The automatic mesh method was used for all the three bodies; the top layer, the rotational volume and the bottom layer. The automatic mesh method uses tetrahedral patch conforming mesh combined with sweep mesh, dependent on the complexity of the geometry [ANSYS Inc, a]. The tetrahedral mesh is robust and precise, and the sweep function makes it a fast algorithm. The hexagonal mesh may demand less computer memory per mesh element but is however not quite as robust.

Sizings The sizings were placed in the areas where the resolution had to be relatively high. There were five sizings placed: Pump inlet, outlet, container, blades and the pool walls.

Table 3: Element Sizes for the Five Sizings.

Location	**Element Size** (m)
Pump Inlet	1e-2
Pump Outlet	1e-2
Container	1e-2
Blades	1e-3
Pool Walls	5e-2

Inflation Layer As described in section 2.7.7 inflation layers should be placed on all relevant walls. In table 4 the locations for the inflation layers, the number of layers and the first thickness length is given.

Table 4: Inflation Layer Location with First Layer Thickness (FLT) and the Number of Layers, N.

Location	**FLT** (m)	**N**
Pool Walls	5e-3	12
Blades	5e-4	7
Container	1e-3	10
Anchoring Discs	1e-3	7
Axle	5e-4	7

The only location with a wall boundary that did not have inflation layers, was the pump inlet and outlet. The reason for this was that the velocity gradients were expected to be much larger along the surface than normal to the surface, and inflation layers are designed to counter the exact opposite. If the inflation layers stretch too long a distance out from the pump outlet, it would not let the flows from the different pipes mix fast enough.

4.1.5 License Cap

It was discovered that the ANSYS license possessed by the University of Life Sciences was an introductory license. This license had a cap on the amount of nodes the solver could solve, which was 512 000 nodes. A dialogue with ANSYS provider EDR & MEDESO associate Martin Holst confirmed that the cap on the solver would make a 3D simulation impossible. After considering several options it was found to be necessary to purchase the 'ANSYS Academic Research CFD' License. An interested party, DEEP RIVER AS, sponsored the purchase of the license.

4.1.6 The End of Experimental Setup A

Due to restrictions from the owners of the pool, Elvebakken Videregående Skole, the experimental setup A could not be used (see also section 4.7). The changes were so big that the

model, mesh and simulation for the experimental setup had to be started from the beginning. Thus the planning of experimental setup B started.

The work done in CFX-pre, CFX, and CFX-post for setup A with the new license were not concluded.

4.2 Experimental Setup B

Deep River AS had constructed a small scale turbine with different dimensions than the computer model that was already produced for setup A. The small scale model that was made for testing in the pool had roughly the same shape as the planned Deep River turbine, but instead of downscaling the original CAD model, the more accurate way would be to create a new CAD model based on the small scale test turbine. By creating the small scale model from scratch in SolidWorks the geometry problems that would have come when importing the .igs file were negated.

The experimental setup B was designed with the same thought process as was done in setup A. The setup is described in the material section and illustrated in figure 8 on page 18.

To be able to get the smallest velocity gradients across the turbine, it was important to moderate the velocity gradients that would come from a simple 90 degree pipe bend. Setup B had a lot shorter distance between pump and pump outlet, making it difficult to keep the flow gradients small. As discussed in section 2.1 and shown in figure 4, the development of velocity gradients in the bends right before the pump outlet had to be avoided. To solve this problem, a nozzle for the pump outlet was designed (see section 4.6.2).

4.2.1 SolidWorks (SW)

To create the new model, the measurements from the experimental model was used. The turbine were dissected into six different pieces. The turbine combined with the pump inlet and outlet then consisted of eight pieces that had to be created and put together.

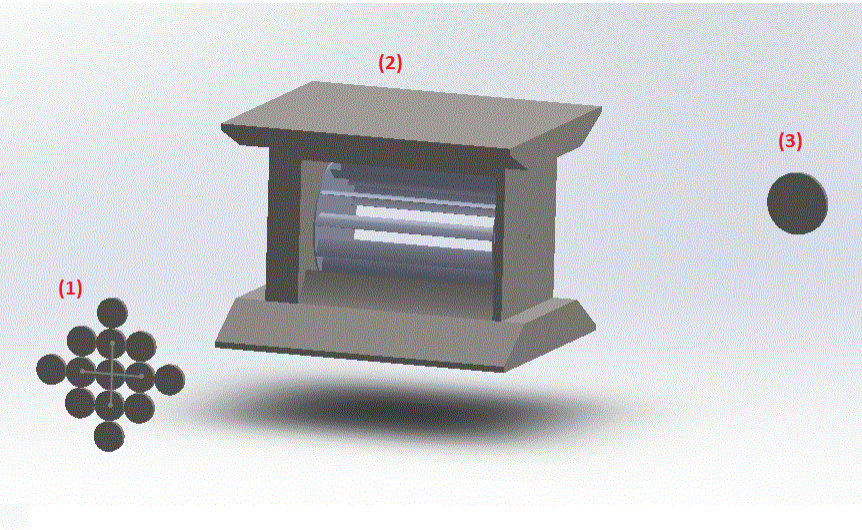

Figure 11: Pump Inlet(1), Turbine(2) and Pump Outlet(3).

Buoyancy platoons, Anchoring Discs, Axle and Pump Inlet All these parts had a simple geometry and were created by drawing a sketch based on the dimensions and extruding it. The dimensions can be seen in materials.

Pump Outlet The geometry in figure 12 does not model nozzle B directly, but corresponds to the measurement locations. There were 13 measurement points that each got a disc with a 24,5 mm radius. The measured value for one point was given as the flow for the area of the corresponding disc. All the discs needed to be inside the area reserved for the pump outlet. Each point had a 50 mm distance between them, so the discs needed to have a slightly smaller radius to cover the most of the area but not connect. They were therefore set to 24.5 mm, giving one millimetre between each disc. The discs could not be connected, because when saved as just one part, the connected surfaces would be shared surfaces, and would then be unable to get individual flow characteristics. This could have been fixed with the DesignModeler feature slice.

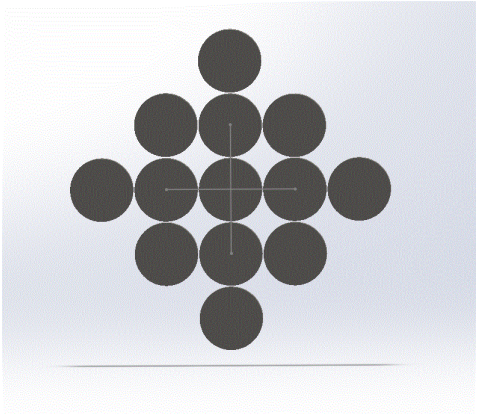

Figure 12: The Pump Outlet

The simplification done here gives that the average flow in one location is the same for the whole area around it within a radius of 24.5 mm.

Turbine Blades The turbine blades were made of thin curved metal plates. Measurements were taken from the small scale turbine, where the thickness length along the blade and from tip to tip, were the important ones. The turbine blades most probably had some small differences that were neglected since it would involve too much work, fine precision measuring and simulation time, probably without affecting the flow conditions significantly. The actual process of creating the blades consisted of producing just one, locking it into the correct place and then use a feature that said the blades should be circularly symmetrical around the axle with a periodicity of 15 degrees. The first one was made the same way as the platoons, drawing a sketch after the measured dimensions and extruding the sketch.

Mating SolidWorks utilizes 'mates' to set terms for how parts can be positioned relative to other parts. Mates were used to lock the parts into their correct position, such as that the platoons should be parallel to the long side of the container and the long ends should

coincide. Placing the mates to lock down a part is pretty straight forward, except for the blades. The blades were locked with 4 mates.

4.2.2 Model Simplification in SolidWorks

Since the model was made from scratch in SW and modelled after the simplified small scale turbine, there were no adjustments necessary before performing the simulation.

4.2.3 ANSYS DesignModeler

The process in the DesignModeler for setup B was similar as for setup A, with some exceptions:

- The positioning of the turbine was moved from the bottom of the pool to 2 cm under the water surface.
- As in setup A, the slice feature was originally used to split the system into two domains (top and bottom layer). But this made trouble for the creation of inflation layers on the pool wall, and was for that reason removed. The slice feature was therefore not used in setup B.

Figure 13 shows how the enclosure feature have been used on the system. There are no solid parts, only two fluid bodies together in a multi-body part.

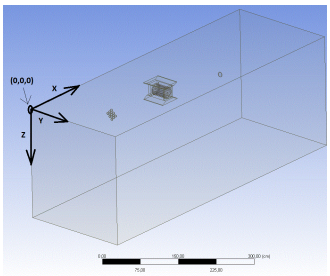

Figure 13: Experimental Setup B as Designed in DesignModeler

(Origo is defined to be in the lower left corner on figure 13)

4.2.4 ANSYS Meshing

Even with the experience of creating the mesh for experimental setup A, there were several challenges when creating the mesh for experimental setup B.

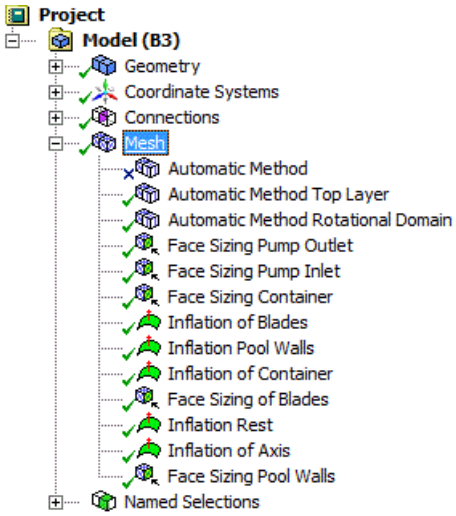

Figure 14: Screenshot of structure list in ANSYS Mesh

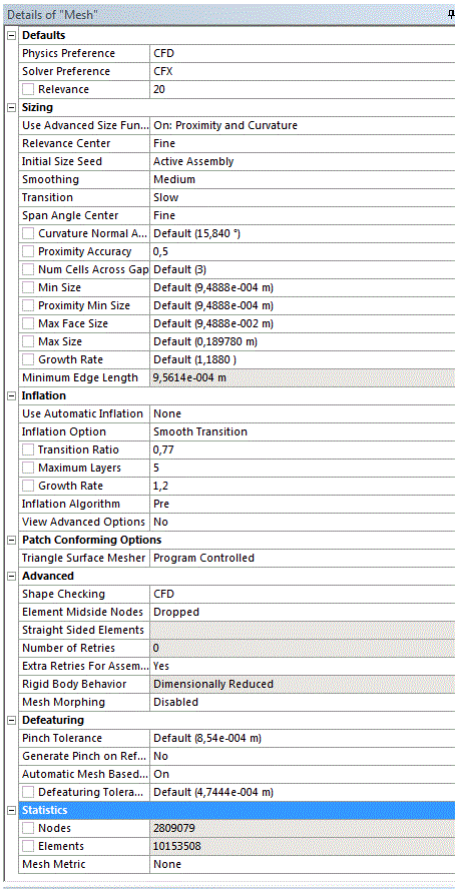

Figure 15: Global Mesh Settings.

Global Mesh Settings The global mesh settings were set as shown in figure 15. Some of the options were left with the default setting, the ones that were not are covered below.

Relevance and Relevance Center Placing fine mesh cells where they were needed and larger mesh cells in areas that were less important was challenging.

Both the relevance and the relevance center affect the mesh element sizes. The relevance setting spans from -100 to +100, and directly affects the global mesh element sizes; the higher the relevance, the smaller the element size. The relevance center is a second setting that manipulates the refinement of the mesh. This setting has three setting options: coarse, medium or fine.

For all geometries there is a difficult balance between fine and coarse mesh. The goal was to get a representative solution as fast as possible. For large geometries it is important to allow less important areas to have a rougher mesh, or the simulation may take a very long time or it may not be solvable. [ANSYS Inc, a, Lecture 5.]

Span Angle Center The span angle center regulate the curvature refinement for edges with the three settings, coarse, medium and fine. The span angle center was set to fine as an attempt to capture the curvature of the blades.

Inflation The global inflation option does not provide the same direct control as the local inflation option, and was therefore deactivated by setting it to 'none'.

Defeaturing length The defeaturing length was actively used when preparing the mesh. The geometry inaccuracies such as two edges not intersecting where they should, but instead creating a small gap, could be overlooked by the mesh generator if they were smaller than the defeaturing length. This made the mesh smooth and whole, without unwanted gaps.

Local Mesh Settings The automatic mesh method was used on the whole system. This was done by specifying the automatic method for the geometry called the top layer and the rotational domain.

Sizings The sizings had the same placements in setup B as in setup A; pump inlet, outlet, container, blades and the pool walls. The size of the elements was however changed since the scale of the turbine was reduced. The sizes of the elements are given in table 5.

Table 5: Element Sizes for the Five Sizings in Setup B.

Location	**Element Size**(m)
Pump Inlet	1e-3
Pump Outlet	1e-3
Container	1e-3
Blades	5e-4
Pool Walls	1e-2

Inflation Layers The placements, first layer thickness and number of layers can be found in table 6. As mentioned in the Design Modeler section above, there were originally problems with the inflation layer crossing from the bottom layer to the top layer. This is illustrated in figure 17.

Illustrations of the inflation layers on different locations can be seen in figure 16.

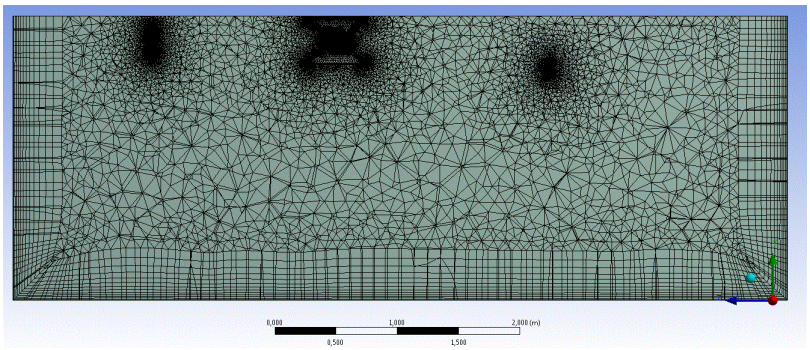

(a) Side view of the generated mesh

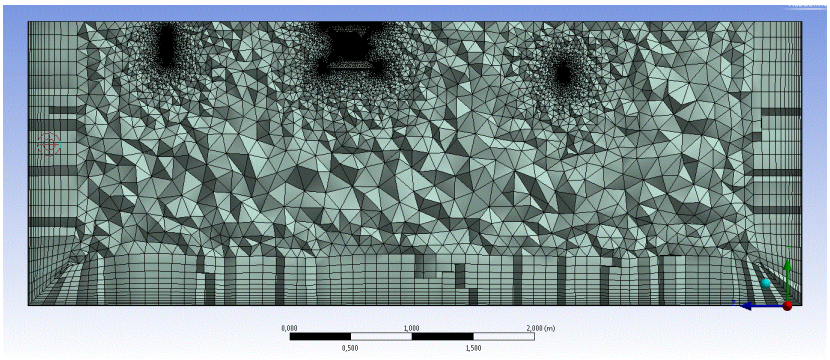

(b) Side view with whole elements

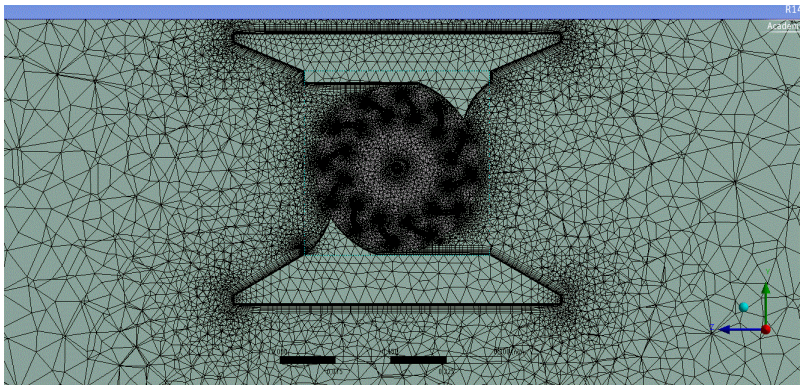

(c) Mesh around the turbine

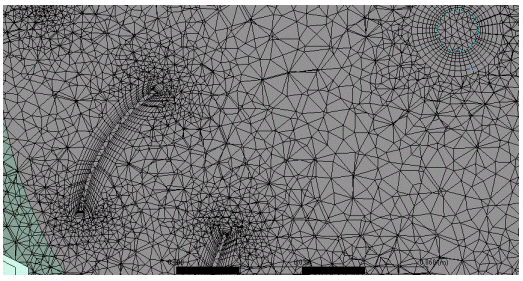

(d) Inflation on blades and axle

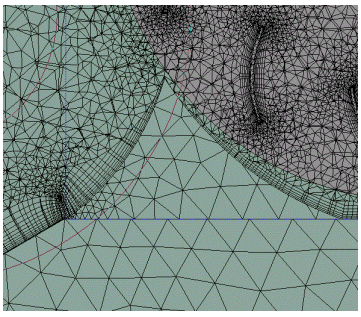

(e) Inflation layers folding together before spoiler

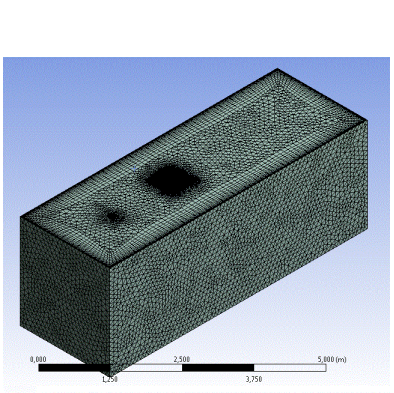

(f) Side view of failed mesh

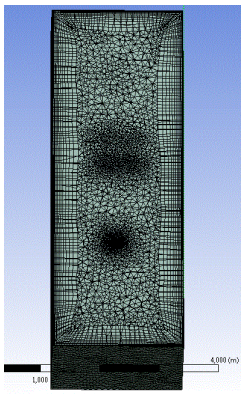

(g) Inflation on blades but not on container

Figure 16: The Generated Mesh

Table 6: Inflation Layer Location with First Layer Thickness (FLT) and Number of Layers, N.

Location	**FLT**(m)	**N**
Pool Walls	5e-3	12
Blades	5e-4	7
Container	1e-3	10
Anchoring Discs	1e-3	7
Axle	5e-4	7

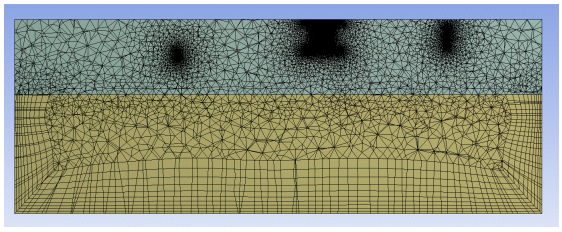

(a) Failed inflation mesh

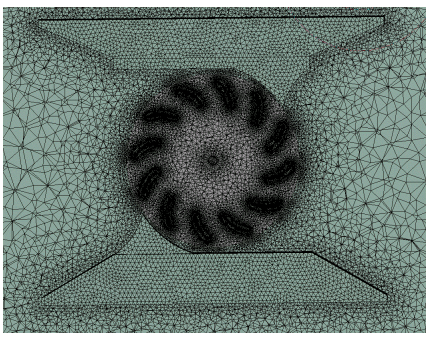

(b) Missing inflation mesh on container

Figure 17: Problem with Inflation

Generating Mesh The mesh generation was not always an easy process. A problem that was encountered was that the mesh was too large for the computer, and the result was that

the computer memory ran out and nothing happened. The only solution to this problem was to reduce the mesh size.

4.2.5 ANSYS CFX-pre

CFX-pre Setup All the actively used settings are listed below. The settings that were not included in the list were the default unchecked options that were not changed.

Analysis Type Transient

Total Time Duration 2s

Time Step 0.05s

Initial Time 0s

Default Domain

Basic Settings

Domain Type Fluid Domain

Material Water

Morphology Continuous Fluid

Reference Pressure 1 atm

Buoyancy Model Non Buoyant

Domain Motion Stationary

Mesh Deformation None

Fluid Models

Heat Transfer None

Turbulence Shear Stress Transport

Wall Function Automatic

Combustion None

Thermal Radiation None

Rotational Domain

Basic Settings

Domain Type Fluid Domain

Material Water

Reference Pressure 1 atm

Buoyancy Model Non Buoyant

Domain Motion Rotating

Angular Velocity $-2.71rpm$

Alternate Rotation Model Check

Mesh Deformation Regions of Motion Specified

Displacement Relative To Previous Mesh

Fluid Models

Heat Transfer None

Turbulence Shear Stress Transport

Wall Function Automatic

Combustion None

Thermal Radiation None

Domain Interface

Basic Settings

Interface Type Fluid Fluid

Interface Side 1

Domain (Filter) Default Domain

Interface Side 2

Domain (Filter) Rotational Domain

Interface Models General Connection

Frame Change/Mixing Model Transient Rotor Stator

Pitch Change None

Solver Control

Basic Settings

Advection Scheme High Resolution

Transient Scheme Second Order Backward Euler

Timestep Initialization Automatic

Turbulence Numerics High Resolution

Convergence Control

Min. Coeff. Loops 1

Max. Coeff. Loops 10

Timescale Control Coefficient Loops

Convergence Criteria

Residual Type RMS

Residual Target $1.E-4$

Output Control Trn Results

Transient Results 1 Standard

File Compression Default

Output Frequency Timestep Interval

Timestep Interval 2

Monitor

Monitor Objects Check

Expression Value $torque_x()@Blades$

The angular velocity were for each simulation taken from the practical experiment (see table **??**).

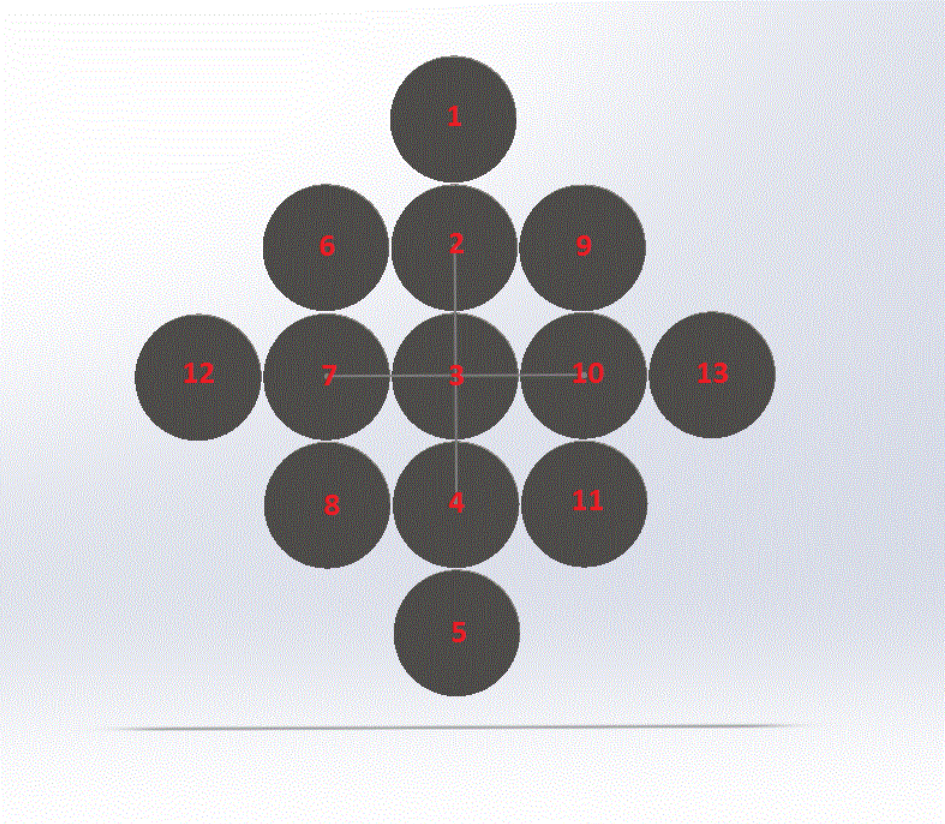

Figure 18: The Modelled Nozzle B with Numbered Outlets

Nozzle B Setup The modelled nozzle consisted of 13 circular discs, each with a radius of 2.45 cm. The distance between each center were five centimetres.

Each of the numbered outlets in figure 18 were given individual outlet settings. The settings were as shown in table 7.

Table 7: Inlet Conditions for Pump Level 3.5.

N_i	**Mass Flow Rate (kg/s)**
1.	0.36
2.	0.37
3.	0.16
4.	0.38
5.	0.03
6.	0.53
7.	0.40
8.	0.40
9.	0.62
10.	0.57
11.	0.40
12.	0.64
13.	0.55

Table 8: Inlet Conditions for Pump Level 6

N_i	**Mass Flow Rate (kg/s)**
1.	0.80
2.	0.81
3.	0.47
4.	0.80
5.	0.13
6.	0.77
7.	0.76
8.	1.05
9.	0.96
10.	0.85
11.	0.88
12.	1.10
13.	0.84

4.3 ANSYS CFX

ANSYS CFX is the solver, and had only settings that would affect the run, not the simulation itself.

4.3.1 Solver Output

The CFX solver gives constant feedback on the residuals in the form of regularly updated graphs. The graphs below are from the ends of the simulated runs. Note that the smooth beginning are from the steady-state simulation, while the jagged part is where the transient simulation begins.

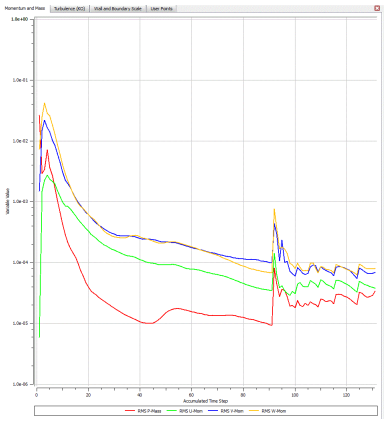

(a) Residuals after run for pump level 3.5.

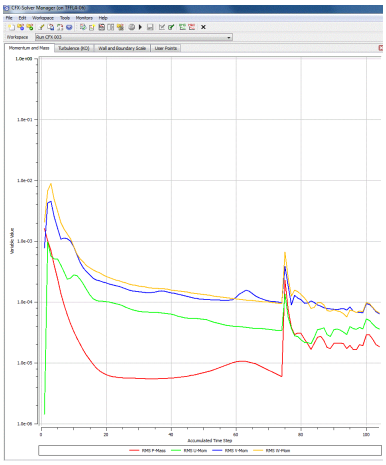

(b) Residuals after run for pump level 6.

Figure 19: Indications from the Solver on Residual Levels

4.3.2 Problems in CFX

When looking for the cause of an error in a run that would not finish, it was found that the memory on the computer was insufficient. Different methods that was thought might solve the problem were tried, but to no avail. It was found necessary to drastically reduce the mesh size for the solver to be able to run the simulation.

4.4 ANSYS CFX-post

In CFX-post it is relatively easy to get a graphic representations of the results from the simulation. Contour planes and planes with vector plots were the most used features, both placed in strategic locations.

4.4.1 Mesh Evaluation

In CFX-pre one may also perform a graphic control on the mesh to e.g, control that the Y^+ value was at the correct levels as shown in figure 20.

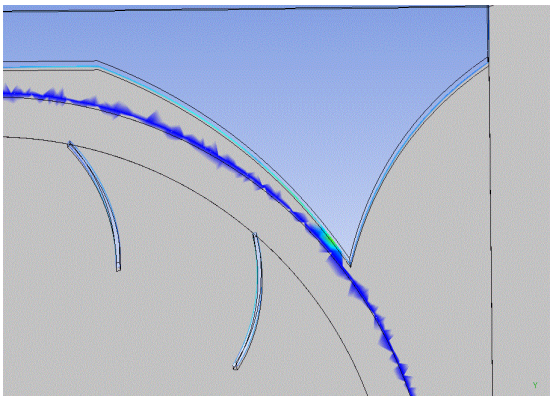

(a) Y^+ on the spoiler

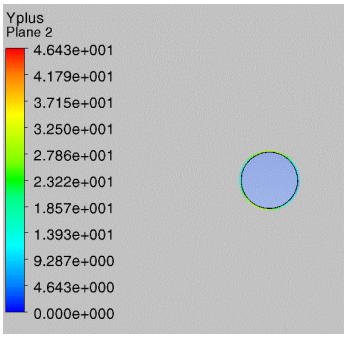

(b) Y^+ on the axle

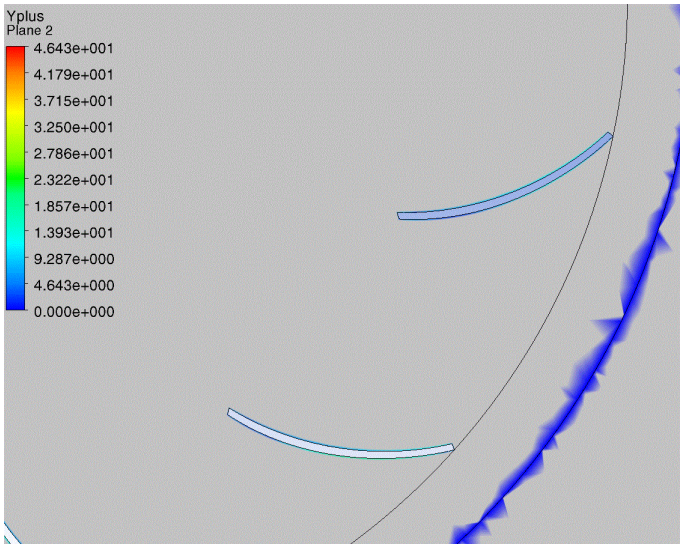

(c) Y^+ on the blades

Figure 20: Graphical Illustration of the Y^+ when using Pump Level 3.5.

The Y^+ values for the different locations can be estimated from figure 20, and is presented numerically in table 9.

Table 9: Y^+ for the Different Locations with Pump Level 3.5.

Location	Y^+
Pool Walls	≤ 15
Blades	$4 \simeq 20$
Spoiler	$13 \sim 15$
Axle	$15 \sim 30$

In single surfaces with very different flow velocities, a large span in the Y^+ values can be observed. An example of this can be seen in figure 20b).

The data of the Y^+ for simulation with pump level 6 were unfortunately not copied before a system update whiped clean the hard drive.

4.4.2 Mesh Dependence

As mentioned in the theory section 2.7.1, an insufficient mesh may affect the simulation results. Tests and changes to the mesh to ensure that the results are mesh independent were not performed. The reduction of mesh elements mentioned in section 4.3.2 gives that the results must be assumed to be mesh dependent.

The figures below show contour planes taken from the simulation results. That the mesh cell is visible in the contour plane speaks for mesh dependent results.

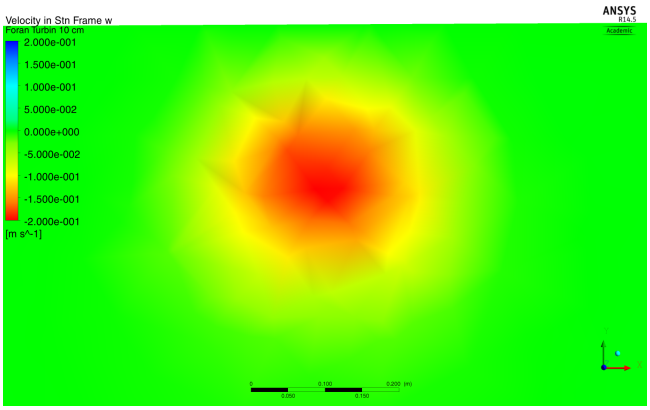

(a) Cross section from location B

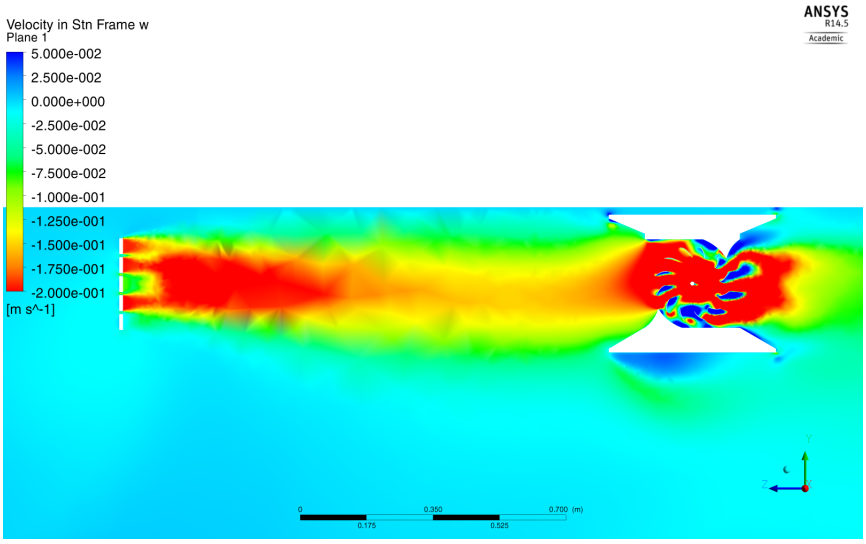

(b) Cross section of pool

Figure 21: Mesh Geometry Visible in Simulation Results

4.5 Measurements from Simulation

To convert the graphical results to numerical data it was necessary to manually interpret the graphic pictures (see appendix) and set values for each measure point. Luckily all the graphic data (pictures of the measured planes) were in the same format. This made it possible to make a semitransparent grid that would position the measure point for each and

every graphic result(see figure 22). Also, the legend was held constant for each pump level.

After this was done, the process of translating the graphical result in one picture into numerical data could begin. This process was followed for all the five planes for both pump level 3.5 and 6, for each time step. Each plane for pump level 3.5 had 58 measure points, and the planes for pump level 6 had 68. For pump level 3.5 the time steps were from 100 to 130, giving 16 time steps. For pump level 6 the time steps were from 82 to 104, giving 12 time steps. All these parameters adds up to 8720 measure points that had to be graphically analysed and the numerical value had to be determined.

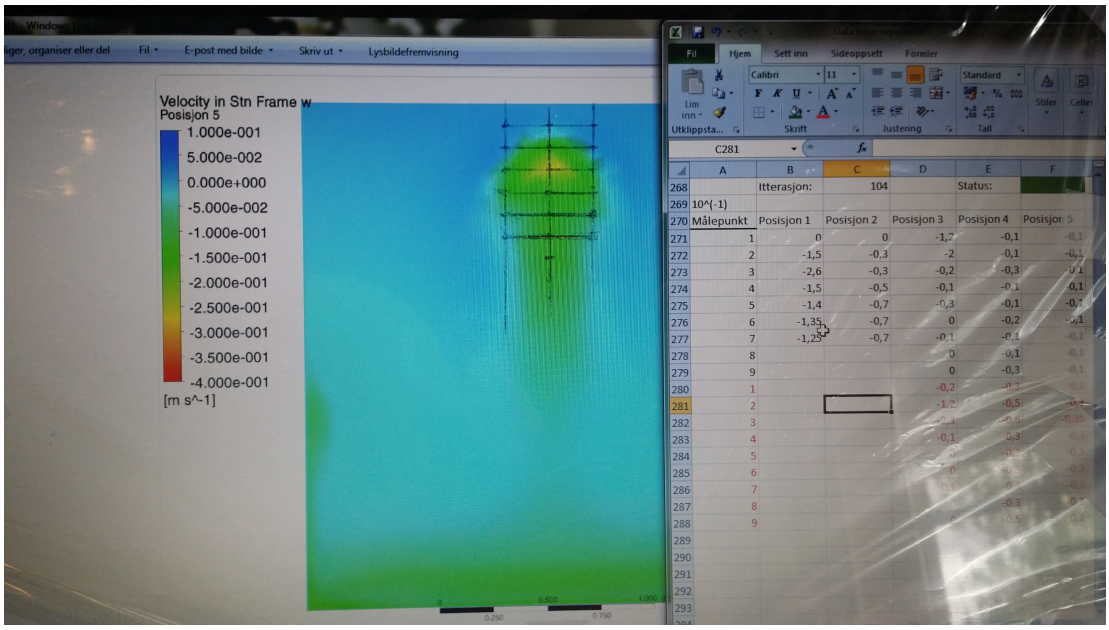

Figure 22: Translating the Graphical Results to Numerical Data

The accuracy for translating the data is estimated to be the quarter of one legend interval. For pump level 3.5 the accuracy was then rounded up to $\pm 1 \cdot 10^{-2} m/s$. For pump level 6 the accuracy were rounded down to $\pm 1 \cdot 10^{-2} m/s$.

4.6 Pump Nozzle

As mentioned earlier in method section 4.1; to minimize the velocity gradients across the turbine generated form the pump and bends in the pipes, a nozzle for the pump outlet was designed.

The nozzle had two requirements that it had to fulfil. The first was to distribute the flow, as evenly as possible, to a surface with the dimensions bigger than the dimensions of the turbine surface. The second requirement was to minimize the velocity gradients coming out of the nozzle. These requirements had to be met and at the same time the nozzle could not build to much into the pool; since it would have restricted the distance the turbine could be from the nozzle (see goal 1 in the method part).

4.6.1 Pump Nozzle A

During the design of the first nozzle it was believed that the pump could be lying on the bottom of the pool as seen in figure 10.

Since the distance from the pump to the pump outlet was quite long, the turbulence generated from the pump was neglected.

When the flow goes from the pump (1) and towards the outlet (2), it is probable that the flow will be quite turbulent. Since the pipes are so long however, the flow might even out a somewhat before the first bend. After the bend the flow will have velocity gradients approximately as seen in figure 4. However, the vertical pipe that goes up towards the pump outlet (2) is relatively long (ca. 2 m), and there might be some turbulence that helps even out the velocity gradients. This makes it plausible that at mid length (3/4 of the distance between (1) and (2)), the velocity gradients would be relatively small. After the half-way-point of the left vertical pipe, the velocity gradients would at some distance from the coming bend change in "preparation" for the bend (see theory section 2.1).

A nozzle that would hinder the flow from developing big velocity gradients in the last bend and let it pump that flow into the pool, needed to be designed . The concept is simple; if one divides water flow into several smaller pipes before the flow have neared a bend (small gradients), the flow in each small pipe will develop velocity gradients, but the flow after the outlet will be much more uniformly distributed. If all the flow was in one pipe it would be like in figure 4 on page 9.

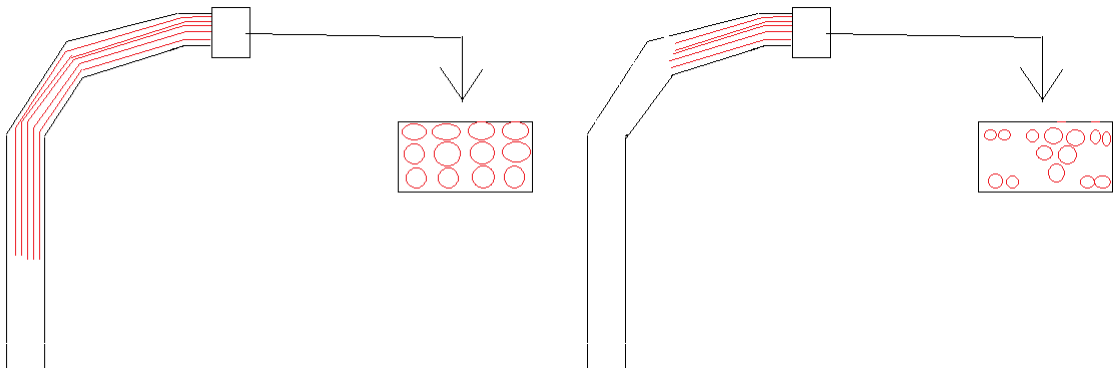

(a) The sketched nozzle design.

(b) The design of the constructed nozzle.

Figure 23: The Sketched Nozzle Design vs. the Buildt Nozzle Design.

The design for the nozzle was sketched roughly as in figure 23a, and consisted of small pipes within a larger pipe like the yellow and green in figure 24. The only exception was that the exit of the small pipes was positioned in the shape of a rectangle. The design was sketched and given to Vestby for construction.

Unfortunately the plans for construction was not followed. The nozzle was constructed with a non-uniform output platform, and the small pipes did not take in water before the flow gradients developed in the bend. The nozzle that was build is shown in figure 23b.

(a) Nozzle A up-side-down.

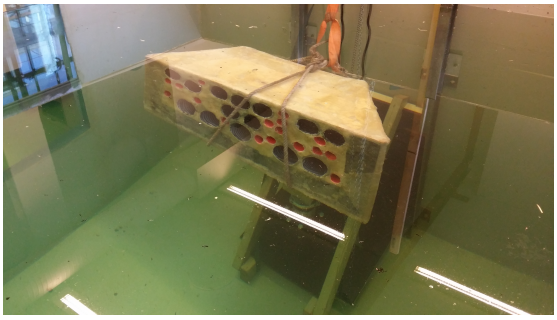

(b) Nozzle A upright in the water.

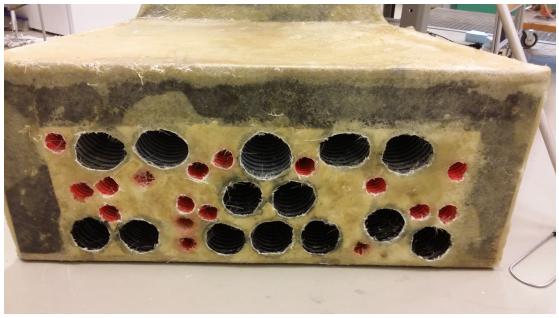

(c) Nozzle A outlet (upside down).

Figure 24: Nozzle A

Actual Performance of Nozzle A Since the design plans was not followed, it was expected that nozzle A would not spread the flow good enough. It was however decided to do an experiment to confirm or falsify this belief. The instrument used are shown in the materials section 3.1 and was placed in a series of locations 0,1 m from each of the larger pipe-outlets, as shown in figure 23. The positions in table 10 and 11 correspond to the positions numbered in figure 24b below.

(a) The instrument 10 cm from the outlet and fastened to the platform.

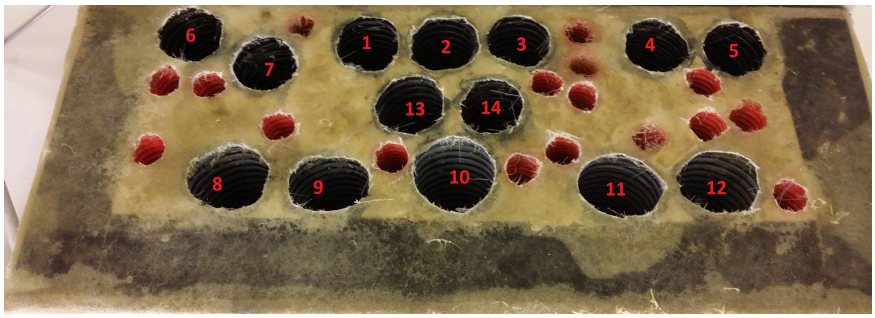

(b) The numbered positions on the nozzle outlet.

Figure 23: Testing the performance of nozzle A.

Table 10: Performance Test of Nozzle A with Pump Level 2.

Measure Point	Average Flow (m/s)	SD (m/s)
1.	0.09	0.32
2.	0.09	0.35
3.	0.12	0.48
4.	0.00	0.00
5.	0.00	0.00
6.	0.00	0.00
7.	0.00	0.00
8.	0.00	0.00
9.	0.00	0.00
10.	0.00	0.00
11.	0.00	0.00
12.	0.00	0.00
13.	0.00	0.00

Table 11: Performance Test of Nozzle A with Pump Level 3.

Measure Point	Average Flow (m/s)	SD (m/s)
1.	0.43	1.52
2.	0.55	1.96
3.	0.40	1.42
4.	0.00	0.00
5.	0.00	0.00
6.	0.00	0.00
7.	0.00	0.00
8.	0.00	0.00
9.	0.00	0.00
10.	0.00	0.00
11.	0.00	0.00
12.	0.00	0.00
13.	0.00	0.00

Actual Performance of Nozzle A - Conclusion From table 10 and 11 above, and figure 24b, it is clear that the flow is only coming out of the three holes in position 1, 2 and 3. Nozzle A did not perform its intended task of evenly spreading the flow.

4.6.2 Pump Nozzle B

The second pump nozzle was built on the same principle as the first nozzle, but this time was the building process closely followed. The changes to the setup considerably reduced the distance between the pump and the pump outlet, and it was therefore necessary to add a part that would speed up the spreading of the water flow from the pump.

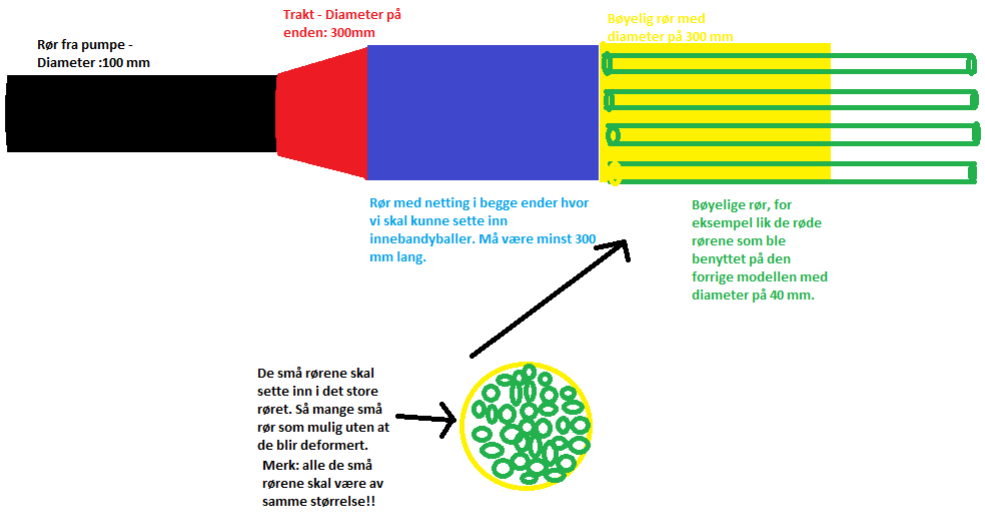

Figure 24: Concept design of pump nozzle B.

Part Description The colors in the description below refer to the colors in figure 24.

Black Pipe out from pump, diameter 0.1 m.

Red Funnel from 0.1 m to 0.3 m.

Blue Contraption for spreading water. Needed to be at least 0.3 m long, and contained floorball balls that was trapped inside the pipe with fences in both ends.

Yellow Pipe with bend, and inside this pipe there will be several smaller pipes (green).

Construction Process The goal when constructing the nozzle was to use inexpensive materials, get the job done quickly, and to make it work.

In figure 25a the topmost part was connected to the pump and the other end was connected to the funnel. The funnel went over to a pipe where each end was sealed with chicken fence and 24 floorball balls filled the inside, as shown in figure 25b. The floorball balls acted as an obstacle for the flow from the pump, which contributed to disperse the flow and reduce the flow gradients after the funnel. The floorball balls were evenly distributed and the goal was to make the flow disperse through the balls without reducing the pressure too much. In figure 25d from the top one can see the pipe that was connected to the pump, the funnel, the flow equalizer and to an adapter for installing the final piece. The pieces did not all fit perfectly, so foam was therefore used in the cracks to reduce the leakage; note that leakage from such a makeshift construction cannot be prevented. Figure 25c, e and f shows the attempt of trying to put the flow in small pipes to avoid the effect as seen in figure 4 in section 2.1. Figure 25g and 25h show the finished nozzle construction. Lastly, the nozzle was oriented towards the turbine and the pump was started.

(a) The funnel and the flow equalizer.

(b) 24 floorballs were insterted to break up the jetstream from the pump.

(c) Nozzle construction site.

(d) All cracks were foamed to prevent leakage.

(e) A 300mm 90 degree bend with 50-60mm pipes inserted.

(f) The space between the small pipes where foamed to keep them together.

(g) Nozzle B connected to the pump.

(h) Nozzle B in the water.

Figure 25: Pump Nozzle Construction Process

The dimensions of the nozzle is described in the materials section 3.3.

4.7 Practical Experiment

Before being able to start the experiment it was necessary to install the pump and pipes that would convert the wave tank to a closed flow circuit.

During the instalment of the pump it was found that the owners of the pool, Elvebakken Videregående Skole, had restrictions as to how the pump could be installed. This change resulted in that the planned setup A could not be used, and a new setup had to be prepared.

Preparing the Setup The process of planing the experiment is covered in section 4.2 on page 26.

A working platform that could span the pool was constructed to make the measuring process easier. Measure instrument A was attached to a lengthening pole that again could be fastened to the platform as seen in figure 7b. The pole itself was marked with lines, indicating at what depth the sensor was, as shown in figure 29a. This made it easier to change vertically from one measure point to another.

(a) Constructing the work platform

(b) Installing the pump

(c) Placing a smoother surface on the platoon surface

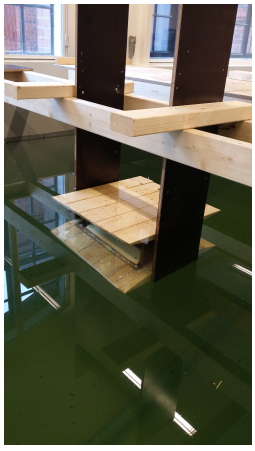

(d) Turbine placed in water

Figure 26: Preparations before Experiment

Changes Along the Way Even though the planning of the experimental setup was completed, there were some unexpected changes along the way.

Until instrument A had proven insufficient, the setup did not have the pipes necessary to reposition the pump outlet from under the pump and to the other side of the pool (see figure 8 on page 18). The flow was pumped towards the turbine, but was also sucked towards the bottom of the turbine. This caused the water to visibly swirl in the pool. This unwanted flow behaviour would jeopardize the experiment since the swirls would be difficult to measure. It was decided that the pipes relocating the pump inlet were necessary for the experiment to proceed.

The pipes took some time to locate but were eventually installed as can be seen in figure 27a. Since the pipe on the bottom of the pool was vibrating, it was tried locked in place along with the pump inlet (see figure 27b). To achieve this the wooden pole was situated so that it pressed down on the vibrating pipe.

(a) The pipe that would relocate the pump inlet

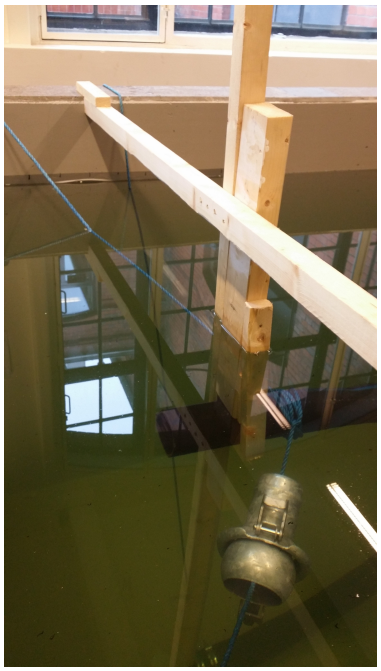

(b) The pump inlet, relocated and fastened

Figure 27: Late Instalments

The owners of the pool, Elvebakken Videregående Skole, made changes to the pool environment at one point by installing an aluminium work platform, see figure 29c. This new platform were difficult to hold in one place, since wheels and no brakes were installed on the platform. By changing the platform, the distance down to the water surface also changed. This needed to be accounted for on the depth markings on the lengthening pole. It was not possible to fasten the rig (see figure 29c) at the very end of the work platform. This could have caused the lengthening pole to tilt outwards from the platform, changing the level of the sensor. This was circumvented by taping a short wooden pole to the rig, thus increasing

(a) Fouling of pump exterior

(b) Unclean water

Figure 28: Fouling in the Pool

the reach to outside the platform. The short wooden pole had to be repositioned each time the sensor needed to be repositioned horizontally.

Fouling As seen in figure 28a and 28b, there were a lot of unwanted materials in the water. As the report by J. A. C. Orme [2001] presented in section 2.2 states, fouling can affect the efficiency of a turbine. This was tried avoided by cleaning the turbine blades and starting the pump soon after.

4.7.1 Performing Measurements

Preparations There were a number of things done before the actual measuring could happen. The list below describes the preparations that was done.

1. The sensor was taped to the lengthening pole. Care was taken to position the sensor with the face normal to the pole.
2. The lengthening pole was marked with lines that indicated the depth of the sensor relative to the vertical center of the turbine.
3. The wooden rig (see figure 29c) was marked with lines indicating the horizontal position of the lengthening pole relative to the center of the turbine.
4. A bubble level was used to ensure the position of the sensor.
5. A measuring tape was used to position the sensor at the appropriate distance from the turbine, so that measurements could be performed in the planned plane.

6. When using the aluminium platform, the rig had to made thicker by using a short wooden pole. See the end of section 4.7.

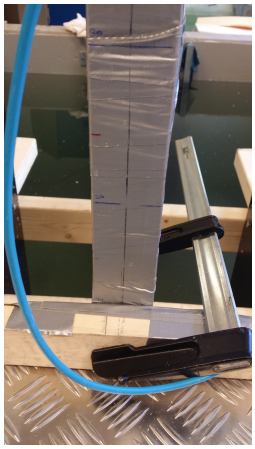

(a) Pole fastened to platform with lines indicating depth

(b) Using a bubble level to ensure correct placement of sensor

(c) Taking measures with instrument B

Figure 29: Performing Measurements

Measure Points It was important to get enough data that a comparison with the simulation would be possible. The decided method was to take five planes that were parallel to the front surface of the turbine, and place a number of measuring points on those planes. This was done for two different pump levels. The planes parallel to the turbine front were positioned like this:

A: 0.5 m from nozzle, 0.1 m from center of turbine.

B: 0.1 m in front of buoyancy platoon, 0.32 m from turbine center.

C: 0.1 m behind buoyancy platoon, 0.32 m from center of turbine.
D: 0.5 m behind buoyancy platoon, 0.72 m from center of turbine.
E: 0.7 m behind buoyancy platton, 0.92 m from center of turbine.

The planes are also illustrated in figure 30; where the first plane on the left is plane A and the one furthest in the back is plane E.

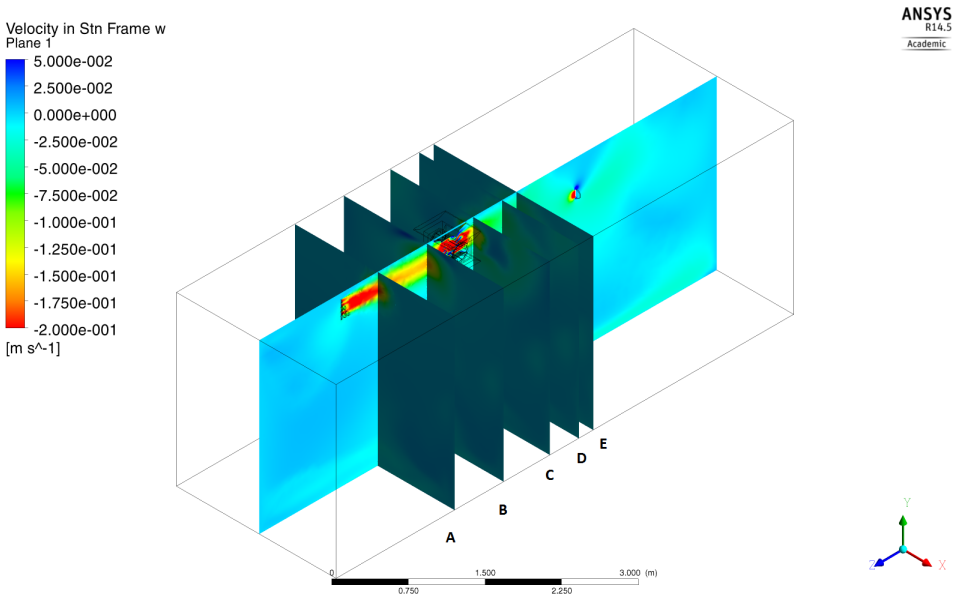

Figure 30: Illustration of the Positions on the Planes that was Measured Upon

Tables 13, 14 and 15 illustrate the different measuring setups that were used when measuring the system. The measuring systems used and for which planes are listed in table 12 below.

Table 12: Used Measuring Setup for the different Planes.

Plane	Pump Level	
	3.5	**6**
A	3	3
B	3	3
C	2	2
D	2	2
E	1	2

*The setup numbers in the table refers to setup 1, 2 and 3 in table 13, 14 and 15

Table 13: Setup 1

			Y:
4	1	7	- 0.10
5	2	8	- 0.20
6	3	9	- 0.30
⌶	⌶	⌶	
X: -20	0	+20	

Table 14: Setup 2

			Y:
4	1	7	- 0.10
5	2	8	- 0.20
6	3	9	- 0.30
13	10	16	- 0.40
14	11	17	- 0.50
15	12	18	- 0.60
⌶	⌶	⌶	
X: -20	0	+20	

Table 15: Setup 3

	Y:
1	- 0.10
2	- 0.20
3	- 0.30
4	- 0.40
5	- 0.50
6	- 0.60
7	- 0.70
⌶	
X: 0	

Measuring the System The pool dimensions are given in the materials section. The dimensions were found using a measuring tape.

Measuring with Instrument A Instrument A (see 'Materials' section 3.1) was used to measure the flow velocity. In the beginning of the measuring process there were no obvious problems with instrument A. After having performed a series of measurements it was found that the sensor would not always indicate a current, even if there visibly was one. This was a real problem since the instrument was not able to measure the current behind the turbine at all.

Another indication that instrument A was not good enough, was when adjusting the pump level. The turbine started spinning at level 4, while the instrument could not measure any flow until level 6. The instrument was then setting the lower limits for the flow velocity, not the turbine. Since the instrument would not measure flow behind the turbine, and no flow velocity when the pump level was lower than level 6, the flow it did measure was not reliable either.

A new sensor was purchased and used with the same log computer as the previous one, but the results were still the same. After these two attempts it became clear that a more accurate instrument was required. Some research on different instrument types was done, which singled out a measuring system; namely instrument B.

Measuring with Instrument B Instrument B, as shown in figure 6 and described in section 3.1, was utilized in the same way as instrument A. The sensor was taped to a lengthening pole that again was fastened to the platform. This is shown in figure 29c. Instrument B performed as expected.

Measuring the Rotational Velocity A piece of grey tape was placed on one of the turbine blades. When the pump level was 3.5, the time were taken for the blade to pass the spoiler 10 times, and this process was repeated 3 times. For pump level 6 the time was taken for the blade to pass the spoiler 20 times, and the process was repeated 5 times.

Table 16: Rotational Velocities

Pump Level	Average (rev/s)	SD (rev/s)
3.5	0.05	0.01
6	0.26	0.01

5 Results and Discussion

5.1 Measurements from Experiment

Accuracy of Instrument B In section 3.1 the accuracy for instrument b is given in equation 2. The "reading" component of that equation may be estimated to be zero for this experiment with such low average values. The "full scale" component of 0.20 m/s however is relatively large. This factor must be taken into consideration when comparing simulation to the experiment, and maybe also experiment with pump level 3.5 with pump level 6.

Since inaccuracy from the instrument is so large, one should look at the curves instead of directly comparing the values.

5.2 Measurements from Simulation

The Modelled System In the case of the simulation performed in this thesis, there have been made some assumptions that, if incorrect, affects the comparability with the experiment. The most controversial assumption is that nozzle B could be modelled by 13 circular discs like shown in figure 18. The modelled nozzle and the actual nozzle are compared in section 5.4.

Accuracy of Graphical Results By taking the converged data with a convergence point of $1 * 10-4$, one ensures highly accurate results within the limits of the simulation. The limits of the simulation are set by the model, the mesh, and the settings in CFX-pre. If either of those components brings an error into the solver, the solver will calculate with that error with a high accuracy (if convergence is reached), but the results will be on the wrong basis.

From Graphical to Numerical Results The added inaccuracy when reading the graphical results and translating them to numerical values was estimated in section 4.5 to be $\pm 0.01 m/s$. The average and standard deviations have been calculated from a sample size of 16 and 12, for pump level 3.5 and 6 respectively.

5.2.1 Evaluation of the Mesh

Inflation Layers and Y^+ Inflation layers have been placed on all boundary conditions defined as walls, except for the inlet and outlet. The first element thickness may be discussed by looking at the criteria for the turbulence model in section 2.8.3 on page 16, and the Y^+ values in table 9 on page 35.

When comparing the criteria for the turbulence model and the values for Y^+, it is clear that the first layer thickness is not optimal in any of the cases. The blades should optimally have a $Y^+ < 2$. The spoiler and axle should be inside the laminar layer at $Y^+ < 10$, while the pool walls could have a first layer thickness that gave $Y^+ = 30 \sim 300$.

Since the mesh used for simulation of pump level 3.5 and pump level 6 were identical, it is unlikely that the surfaces have better Y^+ values(see section 4.4.1.

Mesh Dependent Results As mentioned in section 4.4.2, testing to ensure that the results were mesh independent was not performed. This along with the illustrations in figure 21 gives that the results must be assumed to be mesh dependent.

5.3 Figures from Simulation

The cross section of the pool were captured as images for all the time steps and are presented below in figure 31 and 32. All the figures for each pump level have the same legend. The contours given in the images are of the velocity in z-direction, since this is the component that is measured in the experiment. Note that downstream is in the -z - direction, which is why the red contours are labelled with negative values.

The vector plots which is the (d) figure in both figure 31 and 32 are the only figures that shows velocity in all directions.

5.3.1 Simulated Pump Level 3.5

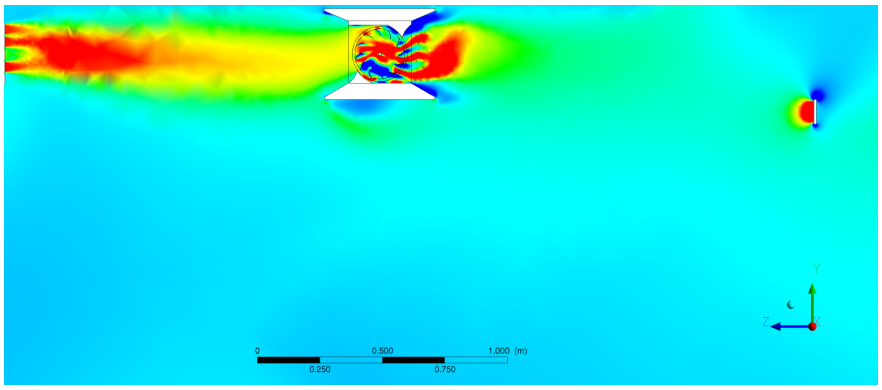

(a)

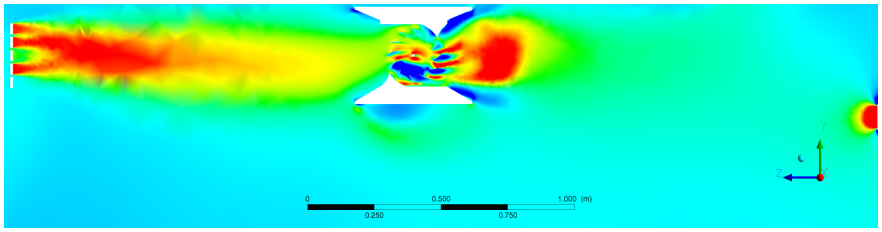

(b)

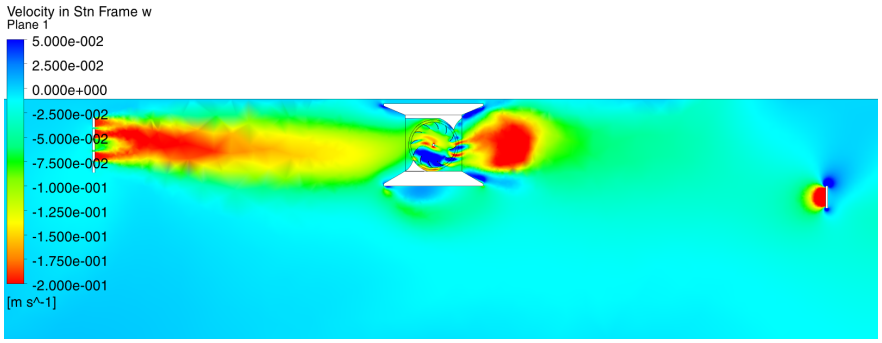

(c)

There are no obvious drastic differences in figures 31(a), (b), and (c), even though the two first are 10 time steps apart and the third an additional six timesteps further. Some changes

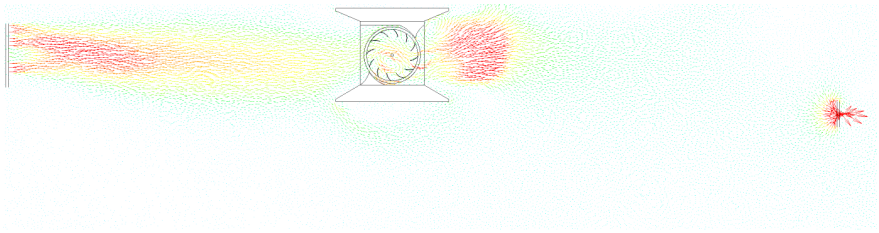

(d)

Figure 31: Cross Section Illustrations from Simulation with Pump Level 3.5.
*All the images have the same legend.

may not be measurable in the experiment, as the changes around the blades caused by the rotating blades. Other changes, like the changed flow characteristics immediately behind the turbine might be measurable in plane C (see figure 30). The amount of changes should then be indicated in the standard deviation.

By looking at figure (d), it seems like most of the flow goes through the turbine, with only a small portion going under.

The pump inlet generated flow are not directed specifically towards the turbine, but rather sucks in flow from the front and surroundings of the inlet surface.

5.3.2 Simulated Pump Level 6

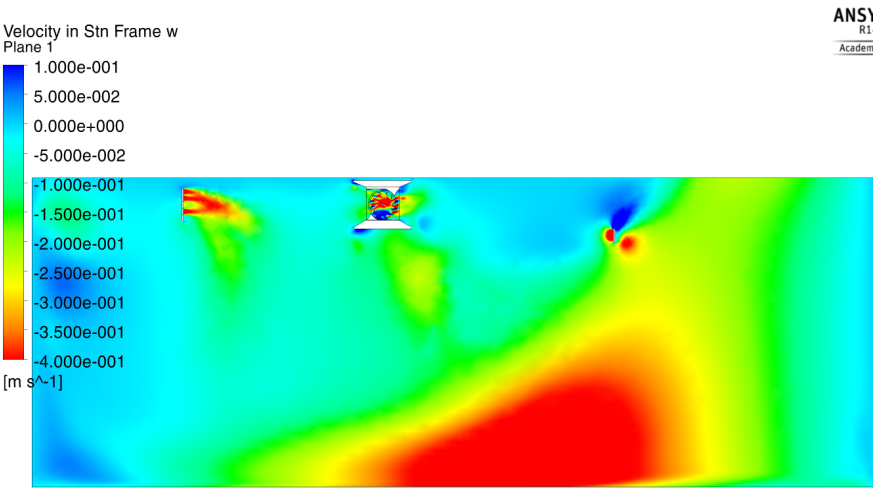

(a)

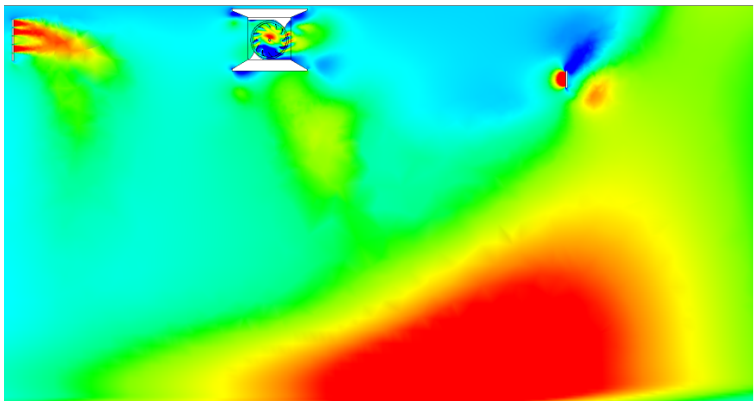

(b)

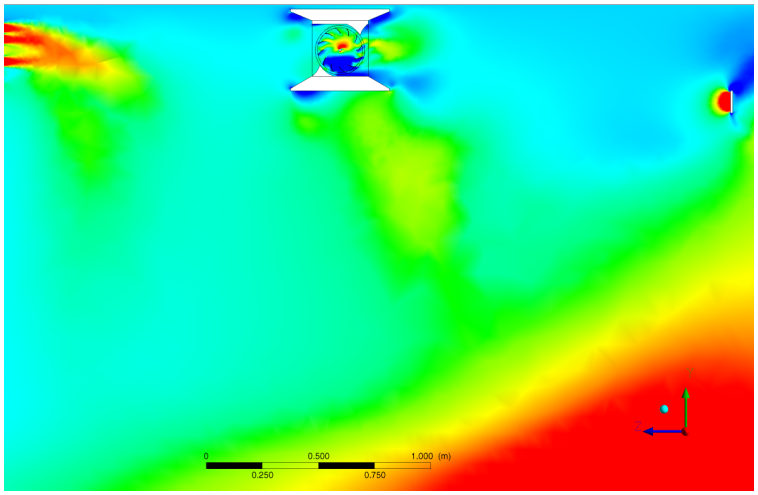

(c)

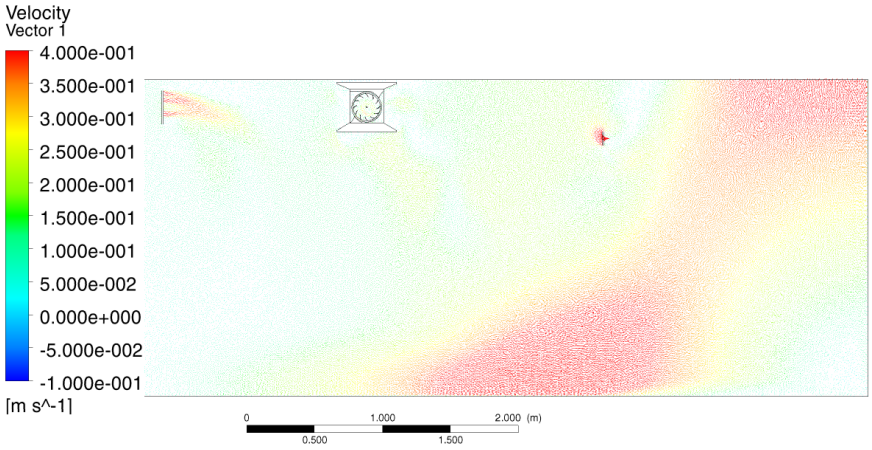

(d)

Figure 32: Cross Section Images from Simulation with Pump Level 6.
*All the images have the same legend.

The figures 32(a), (b), and (c), are all from different time steps (82, 90 and 96 respectively). Some of the largest differences can be seen inside the turbine,and behind the pump inlet. Both locations were not measurable in the experiment.

The differences between figure 32 and figure 31, the simulated results for pump level 3.5 and pump level 6 respectively, are huge. With such differences it must be considered that one of them may be wrong.

It is notable how much stronger the currents are under and behind the pump inlet vs. in front of the pump outlet. There are also no red vectors leading from the pump outlet and towards the bottom. For the flow to gather as shown in these figures, then the flow at the end of the pool must follow the wall horizontally and flow back along the wall.

The water flow is quickly diverted from the turbine and flows along the pool floor to end up behind the pump inlet. This is not the expected flow pattern, and figure 31 must be discussed together with the measure point values in the appropriate planes.

5.4 Actual Performance of Pump Nozzle B

Table 17: Test of Nozzle B with Pump Level 3.5

Measure Point	Average Flow (m/s)	SD (m/s)
1.	0.19	0.01
2.	0.20	0.01
3.	0.09	0.01
4.	0.20	0.01
5.	0.01	0.02
6.	0.28	0.01
7.	0.21	0.01
8.	0.21	0.02
9.	0.33	0.01
10.	0.30	0.01
11.	0.21	0.01
12.	0.34	0.02
13.	0.29	0.01

Table 18: Test of Nozzle B with Pump Level 6.

Measure Point	Average Flow (m/s)	SD (m/s)
1.	0.42	0.02
2.	0.43	0.02
3.	0.25	0.03
4.	0.43	0.01
5.	0.07	0.02
6.	0.41	0.02
7.	0.40	0.01
8.	0.56	0.02
9.	0.51	0.02
10.	0.45	0.01
11.	0.50	0.01
12.	0.58	0.02
13.	0.45	0.02

Table 19: Flow Spread from Nozzle B at Pump Level 3.5

						Y(cm):
		0.19			-	9.5
	0.28	0.20	0.33		-	14.5
0.34	0.21	0.09	0.30	0.29	-	19.5
	0.21	0.20	0.21		-	24.5
		0.01			-	29.5
X(cm):	-10	-5	0	+5	+10	

Table 20: Flow Spread from Nozzle B at Pump Level 6

						Y(cm):
		0.42			-	9.5
	0.41	0.43	0.51		-	14.5
0.58	0.40	0.25	0.45	0.45	-	19.5
	0.56	0.43	0.50		-	24.5
		0.07			-	29.5
X(cm):	-10	-5	0	+5	+10	

As opposed to the first nozzle that was discussed in section 4.6.1, it is evident from table 17 and 18 that nozzle B have managed to spread the water flow. The goal when designing and constructing nozzle B was to spread the flow as uniformly as possible. The standard deviations are small relative to the averages, indicating that the flow out of the nozzle was quite stable.

The measure points 3 and 5 have the values that deviates most from the rest for both pump level 3.5 and 6. measure point 3 is in the center of the nozzle, while measure point 5 is in the center bottom.

By comparing measure points 5, 7, 9, 11 and 12 in both pump level 3.5 and 6, to the rest of the measure points within their pump level, they may seem to have similar flow characteristics. However, the rest of the measure points indicates that the flow characteristics are different.

The difference in flow pattern is probably caused by the changes in flow patterns inside the pump and through the floorball balls when the pump level was changed.

5.5 Performance of the Modelled Nozzle

The goal of the modelled nozzle was to influence the modelled system in the same way the actual nozzle affected the real system.

To evaluate if the modelled nozzle performed as hoped, it is necessary to look at the flow patterns some distance away from the nozzle, and then compare it to the actual flow pattern. This comparison is included in the following section where the simulation and experiment is compared for all locations.

5.6 Comparison of Experiment and Simulation, Pump Level 3.5

The following tables show the time averaged flow velocity values for the respective pump levels, planes and measure points. The standard deviations(SDs) may be an indication for the accuracy of the measurements, but may also depict the transient variations in the flow.

From Experiment
Table 21: Location A, Pump Level 3.5.

Measure Point	Average Flow (m/s)	SD (m/s)
1.	0.20	0.00
2.	0.19	0.01
3.	0.01	0.02
4.	0.00	0.00
5.	0.00	0.00
6.	0.00	0.00
7.	0.00	0.00

From Simulation
Table 22: Location A, Pump Level 3.5.

Measure Point	Average Flow (m/s)	SD (m/s)
1.	0.10	0.01
2.	0.20	0.01
3.	0.11	0.01
4.	0.02	0.00
5.	0.01	0.03
6.	0.00	0.00
7.	0.00	0.00

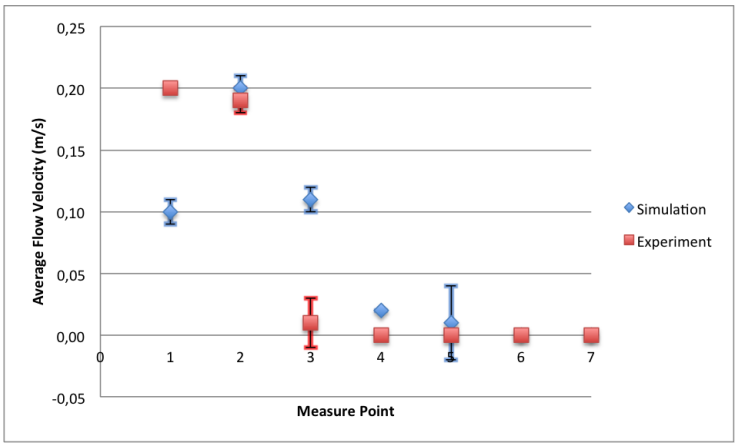

Figure 33: Simulation vs. Experiment for Location A, Pump Level 3.5.

Location A is far enough away from the nozzle that there should have been some mixing in the currents, but also close enough so that the flow patterns should be recognizable. From figure 33 it is clear that there are already notable differences in the effect from the real nozzle and the modelled nozzle. For the difference to already be this prominent there must be a weakness with the model. One explanation may be that the direction of the flow exciting the real nozzle may be tilted upwards. This would explain the higher experimental value at measure point 1, the even value for measure point 2, and the sudden drop to almost zero in measure point 3. The reduced dispersion of flow at measure points 4 and 5 also supports the tilted nozzle theory.

The simulated values from the modelled nozzle do, when taking a look at table 17, fall in line with what would be expected of a water flow from a non-tilted real nozzle in plane A.

The SDs are relatively small, indicating that there were small variations in the measurements.

From Experiment

Table 23: Location B, Pump Level 3.5.

Measure Point	Average Flow (m/s)	SD (m/s)
1.	0.16	0.01
2.	0.14	0.03
3.	0.04	0.04
4.	0.01	0.01
5.	0.00	0.00
6.	0.00	0.00

From Simulation

Table 24: Location B, Pump Level 3.5.

Measure Point	Average Flow (m/s)	SD (m/s)
1.	0.06	0.01
2.	0.13	0.01
3.	0.11	0.01
4.	0.05	0.00
5.	0.02	0.00
6.	0.02	0.00

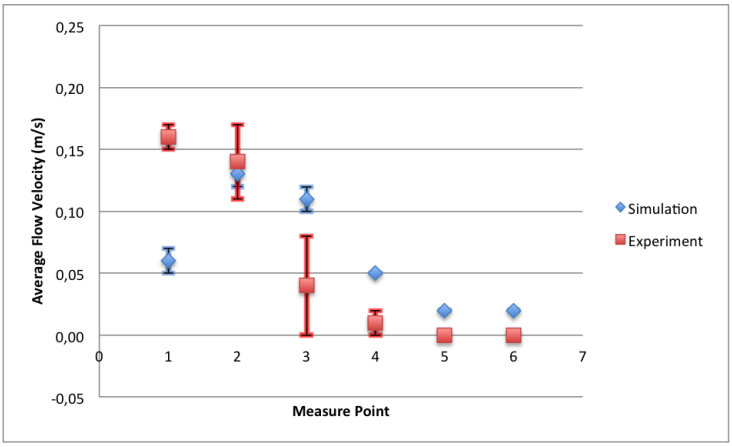

Figure 34: Simulation vs. Experiment for Location B, Pump Level 3.5.

Plane B is located 10 cm from the front of the buoyancy platoon, and the current will at this point be affected by the turbine.
If the assumption from plane A is true, that the real turbine is tilted, then it should be possible to find indications of this also in plane B.
When comparing the graphs in figure 33 with the graphs in figure 34, they seem to be following a closely related curve. Further, the higher indicated flow velocity value for the experiment in measure point 1, and the lower value in measure point 3, both follow the pattern that would be expected if the real nozzle was tilted.

The simulation indicates that from plane A to plane B there have been an increased dispersion of flow, which have increased the indicated velocities at measure points 4 and 6. Measure point 5 in plane B does not have a significantly different value than in plane A.

From Experiment

Table 25: Location C, Pump Level 3.5.

Measure Point	Average Flow (m/s)	SD (m/s)
1.	0.01	0.02
2.	0.09	0.01
3.	0.05	0.03
4.	0.00	0.00
5.	0.00	0.00
6.	0.00	0.00
7.	0.05	0.03
8.	0.05	0.03
9.	0.04	0.03
10.	0.00	0.00
11.	0.00	0.00
12.	0.00	0.00
13.	0.00	0.00
14.	0.00	0.00
15.	0.00	0.00
16.	0.00	0.00
17.	0.00	0.00
18.	0.00	0.00

From Simulation

Table 26: Location C, Pump Level 3.5.

Measure Point	Average Flow (m/s)	SD (m/s)
1.	0.13	0.03
2.	0.17	0.04
3.	0.11	0.04
4.	0.00	0.00
5.	0.00	0.01
6.	0.02	0.01
7.	0.00	0.01
8.	0.01	0.03
9.	0.02	0.01
10.	0.03	0.00
11.	0.03	0.00
12.	0.03	0.00
13.	0.04	0.01
14.	0.04	0.01
15.	0.03	0.00
16.	0.04	0.01
17.	0.03	0.01
18.	0.03	0.00

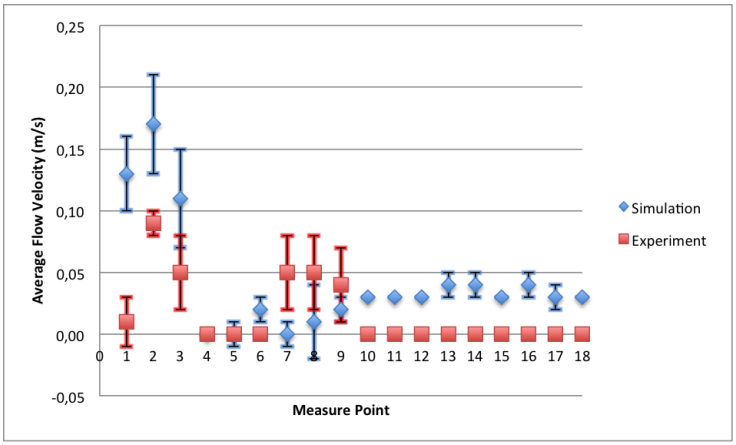

Figure 35: Simulation vs. Experiment for Location C, Pump Level 3.5.

The first three measure points seem to have a similar curve, where in both simulation and experiment the velocity has the highest value in measure point 2, with lower values in

measure points 1 and 2. The curve of the graph from the experiment are not identical to the graph from the simulation, but they do have similarities.

It might be that since the flow from the nozzle seem to be tilted upwards, that a larger part of the flow would go over the turbine than indicated in the simulation. However, even if it was certain that some portion of the flow escaped over the turbine, it could not be said conclusively that it caused the lower average in measure point 1 behind the turbine.

When looking in figure 31a one can see that the flow is accelerated through the turbine, and the back spoiler along with the blades presses the flow out the bottom half of the turbine. Figure 31b however have a different blade placement and the exciting flow is more dispersed. The changes in the exciting flow as an effect of the rotating blades is found in the numerical data as the higher SD values.

Plane C is the first plane where measure points also were placed horizontally, and in figure 35 the experimental graph indicate an asymmetrical dispersion of the flow horizontally. The measure points on the left of the center, 4-5-6, does not indicate any flow while the measure points on the right, 7-8-9, does indicate a flow. The simulation indicates values for the right and left side that are similar but with some differences between measure point 5 and 8.

The turbine does little to promote horizontal changes in the flow, and is therefore a unlikely cause of the observed differences. When looking at figure 25g on page 40, it can be seen that all the inner pipes does not only follow the curve of the larger outer pipe, but they also curve to some degree among themselves. This may cause the water flow to have a x-directional component, which may cause the observed effect. Even if the curve of the inner pipes did not cause the horizontal differences, a small angular displacement of the nozzle would give the same effect.

All the measurements in the experiment at greater depths than measure points 3, 6, and 9, indicate no flow at all. The simulation however have a relatively well dispersed stable flow at those depths. This difference may also be explained by a vertically tilted nozzle. The flow exciting the nozzle would then be aimed to some degree upwards, which could hinder the dispersion of flow to the region under the turbine.

From Experiment

Table 27: Location D, Pump Level 3.5.

Measure Point	Average Flow (m/s)	SD (m/s)
1.	0.05	0.03
2.	0.07	0.02
3.	0.04	0.03
4.	0.00	0.00
5.	0.00	0.00
6.	0.00	0.01
7.	0.02	0.03
8.	0.01	0.02
9.	0.00	0.00
10.	0.00	0.02
11.	0.00	0.00
12.	0.00	0.00
13.	0.00	0.00
14.	0.00	0.00
15.	0.00	0.00
16.	0.02	0.03
17.	0.00	0.00
18.	0.00	0.01

From Simulation

Table 28: Location D, Pump Level 3.5.

Measure Point	Average Flow (m/s)	SD (m/s)
1.	0.05	0.01
2.	0.06	0.00
3.	0.05	0.00
4.	0.02	0.00
5.	0.02	0.00
6.	0.02	0.00
7.	0.02	0.00
8.	0.04	0.01
9.	0.04	0.01
10.	0.03	0.00
11.	0.02	0.00
12.	0.02	0.00
13.	0.03	0.00
14.	0.03	0.00
15.	0.02	0.00
16.	0.03	0.00
17.	0.03	0.00
18.	0.02	0.00

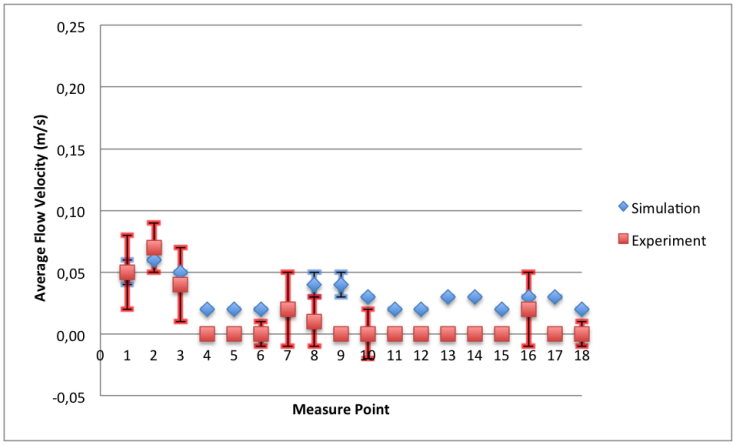

Figure 36: Simulation vs. Experiment for Location D, Pump Level 3.5.

Plane D is 0.72 metre behind the center of the turbine, and the graphs in figure 36 indicate that the flow velocities have levelled some when compared to the velocities in plane C. The same indications can be seen from figure 31a.

The differences between the experimental and simulated results are small for the three first measure points. However, the experimental flow seem still to be leaning upwards and to the right.

The simulation have symmetrical results for measure points 13-14-15 and 16-17-18, but not for 4-5-6 and 7-8-9. The latter measure points were expected to be symmetrical. The outer measure points are placed at the side edge of the turbine, and when looking at figure 9 on page 19 one can see that the left wall is thicker than the right wall. In retrospect the symmetry line should have been placed in the center of the turbine wheel, not the turbine itself. An off-centred symmetry line might explain the differences in the measure points on the top left and right side.

From Experiment

Table 29: Location E, Pump Level 3.5.

Measure Point	Average Flow (m/s)	SD (m/s)
1.	0.07	0.02
2.	0.04	0.03
3.	0.03	0.03
4.	0.00	0.00
5.	0.00	0.01
6.	0.00	0.00
7.	0.01	0.02
8.	0.02	0.03
9.	0.02	0.03

From Simulation

Table 30: Location E, Pump Level 3.5.

Measure Point	Average Flow (m/s)	SD (m/s)
1.	0.05	0.01
2.	0.06	0.01
3.	0.05	0.01
4.	0.02	0.00
5.	0.02	0.00
6.	0.03	0.00
7.	0.02	0.00
8.	0.04	0.01
9.	0.04	0.00

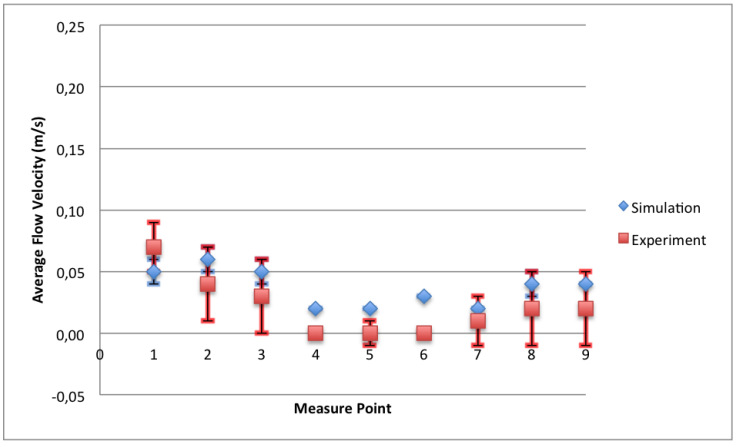

Figure 37: Simulation vs. Experiment for Location E, Pump Level 3.5.

The three first measure points in plane E, as shown in figure 37, are on average a little smaller than the three first measure points in plane D(see figure 36). This may indicate the continuation of the flow dispersion. Further, the deeper placed measure points now have higher velocity than before, which may indicate that the suction from the pump inlet has started taking effect.

The results from the simulation is not symmetrical in this plane either, and the experimental results indicates the same as before; a flow on the right and only a minuscule flow variation with zero as average (see table 29) on the left.

5.7 Comparison of Experiment and Simulation, Pump Level 6

The following tables show the time averaged flow velocity values for the respective pump levels, planes and measure points. The standard deviations(SDs) may be an indication for the accuracy of the measurements, but may also depict the transient variations in the flow.

From Experiment

Table 31: Location A, Pump Level 6.

Measure Point	Average Flow (m/s)	SD (m/s)
1.	0.48	0.01
2.	0.45	0.02
3.	0.11	0.05
4.	0.00	0.00
5.	0.00	0.00
6.	0.00	0.00
7.	0.00	0.00

From Simulation

Table 32: Location A, Pump Level 6.

Measure Point	Average Flow (m/s)	SD (m/s)
1.	0.01	0.01
2.	0.13	0.02
3.	0.25	0.01
4.	0.16	0.02
5.	0.13	0.02
6.	0.12	0.01
7.	0.12	0.01

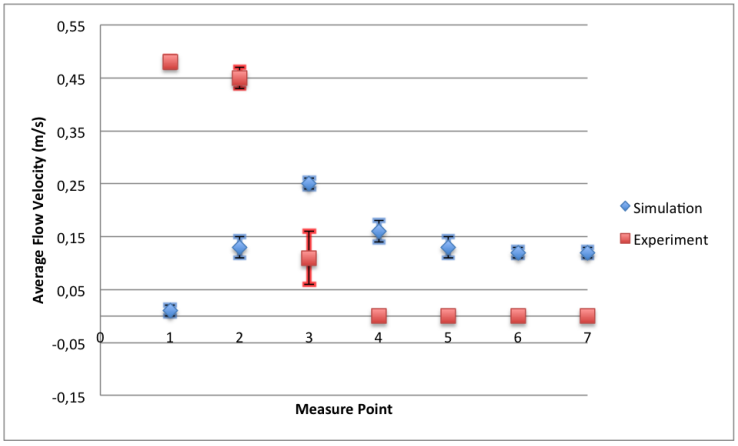

Figure 38: Simulation vs. Experiment for Location A, Pump Level 6.

For plane A which, is only 0.50 metre from the nozzle, the differences shown in figure 38 is quite large. For pump level 3.5 it was discussed if the water flow exciting the real nozzle may have a vertical upward velocity component. When looking at table 18 that illustrates the measured flow velocities at the outlet, one can see that the top of the nozzle has a lower velocity (0.41 m/s) than measure point 1 (0.48 m/s) in plane A has. Measure point 1 and the top of the nozzle are at approximately the same depth and would be expected to have close to the same value in plane A. The high velocity values for the two first points and the sudden drop at the lower points indicates that the nozzle is tilted backwards to some degree for this pump level also.

The simulation results in figure 38 is best looked at in tandem with the images in figure 32. It is immediately clear from figure 32a that this is a whole other case than what happened at pump level 3.5 which is shown in figure 31. Before the flow reaches plane A it has, to a large degree, changed direction downwards. Why this direction change has happened in the simulation is not easily discernible. The model used in the simulation with pump level 6 was identical to the one with pump level 3.5 with exception of the rotational velocity of the turbine wheel, and the mass flow of the inlet and outlet.

It should be considered that the simulated flow from the nozzle might be unable to sufficiently penetrate the turbine, and therefore is redirected downwards. This might explain the redirected flow as seen between the nozzle and turbine in figure 32d. However, the relatively large region with high velocity flow at the bottom of the pool and behind the pump inlet can not immediately be explained with that theory.

From Experiment

Table 33: Location B, Pump Level 6.

Measure Point	Average Flow (m/s)	SD (m/s)
1.	0.37	0.05
2.	0.33	0.06
3.	0.07	0.05
4.	0.12	0.05
5.	0.02	0.03
6.	0.00	0.00
7.	0.00	0.00

From Simulation

Table 34: Location B, Pump Level 6.

Measure Point	Average Flow (m/s)	SD (m/s)
1.	0.02	0.02
2.	0.03	0.00
3.	0.03	0.01
4.	0.05	0.01
5.	0.07	0.01
6.	0.06	0.01
7.	0.07	0.01

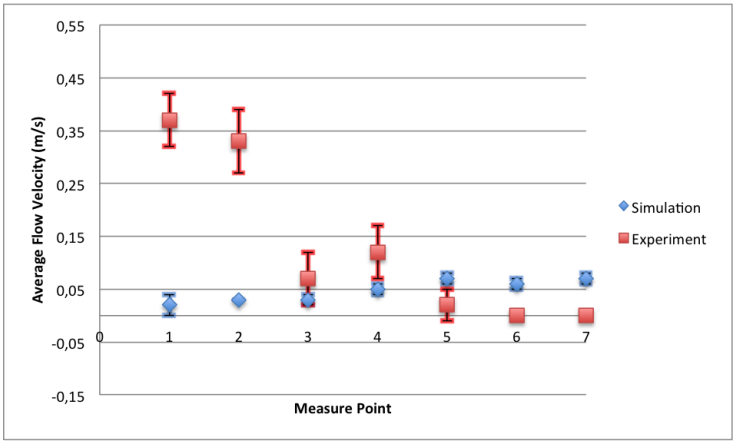

Figure 39: Simulation vs. Experiment for Location B, Pump Level 6.

The graph for the experimental values in figure 39 follows the pattern from the graph in figure 38 with some smaller changes. The peak value for measure points 1, 2 and 3 are lower, while the flow at measure points 4 and 5 have increased. This is most likely cause by dispersion. There is still no indicated flow at measure point 6 or 7.

The simulated results shown in figure 39 seem to increase as the depth is increasing. This is consistent with the images shown in figure 32, but not with the experiment. The values in the graph may be explained by figure 32, but it is still not possible to say conclusively why the current have been diverted. The peak flow seems to be at an even deeper point than measure point 7, or most of the current have been diverted from an z-direction to a x- or y-direction.

From Experiment

Table 35: Location C, Pump Level 6.

Measure Point	Average Flow (m/s)	SD (m/s)
1.	0.01	0.03
2.	0.11	0.04
3.	0.13	0.04
4.	0.00	0.00
5.	0.07	0.04
6.	0.13	0.02
7.	0.11	0.03
8.	0.11	0.02
9.	0.11	0.03
10.	0.01	0.02
11.	0.00	0.00
12.	0.00	0.00
13.	0.01	0.03
14.	0.00	0.00
15.	0.00	0.00
16.	0.05	0.03
17.	0.00	0.00
18.	0.00	0.00

From Simulation

Table 36: Location C, Pump Level 6.

Measure Point	Average Flow (m/s)	SD (m/s)
1.	0.11	0.01
2.	0.15	0.02
3.	0.01	0.02
4.	0.02	0.01
5.	0.02	0.01
6.	0.01	0.01
7.	0.02	0.01
8.	0.02	0.01
9.	0.01	0.01
10.	0.02	0.01
11.	0.14	0.01
12.	0.25	0.02
13.	0.02	0.01
14.	0.00	0.00
15.	0.01	0.01
16.	0.01	0.00
17.	0.01	0.01
18.	0.00	0.00

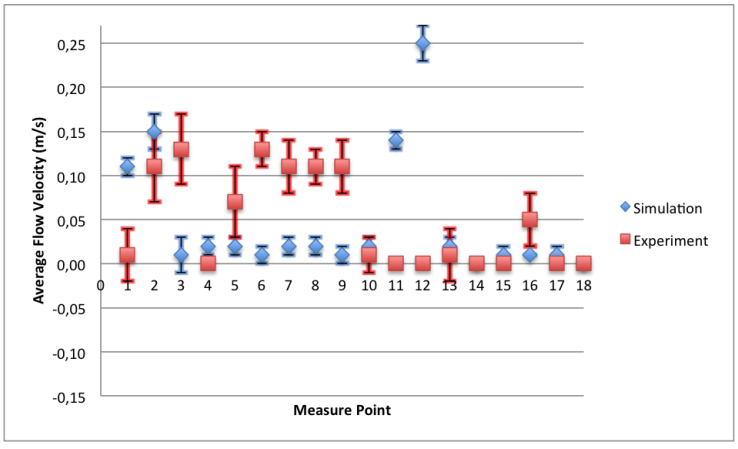

Figure 40: Simulation vs. Experiment for Location C, Pump Level 6.

The experiment do largely follow the expected curve that was observed when the pump level was set to 3.5. The differences is seen in measure points 5 and 6, where these indicate

a flow in the upper left region. Measure points 10-13-16 do all indicate water flow, which they did not for pump level 3.5.

Measure points 1 and 4 do both have an average of zero, but measure point 7, which is at the same depth only further to the right, have an average of 0.11. This may be caused by flow passing on the outside of the turbine, and may also explain why the measure points 7-8-9 is so even. If this is the case when the pump level is set to 6, it should also be considered for pump level 3.5.

The simulation did indicate a flow in measure points 1 and 2, but when looking at figure 32a and 32d it is not obvious where the flow current is coming from. An hypothesis is that the current is generated by the rotating turbine, instead of the turbine being driven by the current. The flow indicated with blue inside the turbine in figure 32c is oriented in the positive z-direction, opposite the flow exciting the nozzle. The blue flow inside the turbine strengthens the belief that the mentioned hypothesis is correct.

The simulation results in measure points from 3 to 10 are all small, and that the measure points 4, 5, 7 and 8 does not approach near to the values seen in measure point 1 and 2 is odd. The oddity comes from the hypothesis mentioned above, if the turbine wheel is the single force driving the current, then the current should be close to uniform along the length of the blades. Some dispersion might be expected, but not at the level seen in figure 40.

The peak values seen in measure points 11 and 12 indicate a high velocity flow under the turbine in the center position. On each side of this flow there are only indications of a small water current.

From Experiment

Table 37: Location D, Pump Level 6.

Measure Point	Average Flow (m/s)	SD (m/s)
1.	0.05	0.03
2.	0.07	0.04
3.	0.12	0.03
4.	0.02	0.04
5.	0.07	0.04
6.	0.07	0.03
7.	0.07	0.04
8.	0.03	0.03
9.	0.03	0.04
10.	0.09	0.02
11.	0.02	0.03
12.	0.00	0.00
13.	0.00	0.00
14.	0.00	0.00
15.	0.00	0.00
16.	0.13	0.03
17.	0.04	0.04
18.	0.00	0.00

From Simulation

Table 38: Location D, Pump Level 6.

Measure Point	Average Flow (m/s)	SD (m/s)
1.	0.01	0.00
2.	0.01	0.00
3.	0.03	0.00
4.	0.01	0.00
5.	0.01	0.00
6.	0.02	0.00
7.	0.01	0.00
8.	0.01	0.00
9.	0.02	0.01
10.	0.03	0.00
11.	0.04	0.01
12.	0.05	0.01
13.	0.03	0.00
14.	0.03	0.00
15.	0.03	0.01
16.	0.03	0.00
17.	0.03	0.00
18.	0.03	0.01

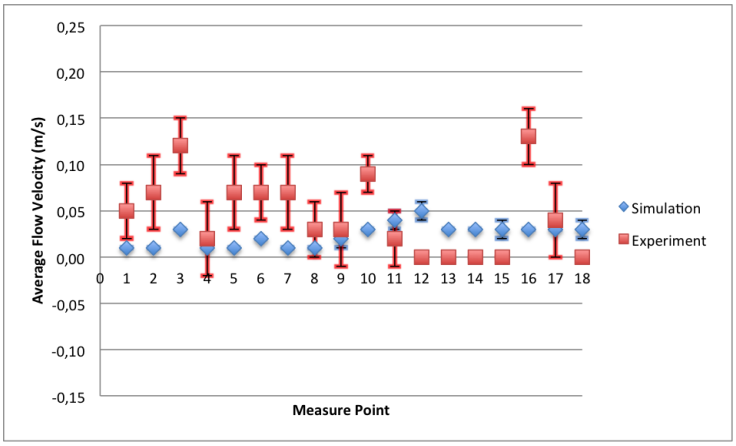

Figure 41: Simulation vs. Experiment for Location D, Pump Level 6.

The simulated results seen in figure 41, are even and stable for all measure points in plane D. This indicates that there are no main current flows inside the measuring area.

The experimental results have higher average flow velocities for increasing depths in the first three measure points. The measure points on the upper left (4-5-6) almost follow the curve set by the center points, while on the right side (7-8-9) there is a decrease in average flow velocity with an increase in depth. This asymmetrical flow behaviour might be caused by a swirl or a secondary current increasing the dispersion of flow on the right side. The relatively high SDs of at these measure points support the plausibility of swirls or a secondary current.

The increased averages in measure points 10, 11, 16 and 17 might be caused by some dispersion of flow from the higher levels (measure points 6 and 9), or being accelerated towards the pump inlet.

From Experiment

Table 39: Location E, Pump Level 6.

Measure Point	Average Flow (m/s)	SD (m/s)
1.	0.08	0.02
2.	0.10	0.02
3.	0.11	0.01
4.	0.04	0.03
5.	0.05	0.03
6.	0.07	0.03
7.	0.09	0.03
8.	0.02	0.03
9.	0.07	0.04
10.	0.08	0.02
11.	0.01	0.03
12.	0.01	0.03
13.	0.00	0.00
14.	0.00	0.00
15.	0.00	0.00
16.	0.05	0.03
17.	0.04	0.05
18.	0.00	0.00

From Simulation

Table 40: Location E, Pump Level 6.

Measure Point	Average Flow (m/s)	SD (m/s)
1.	0.01	0.00
2.	0.01	0.00
3.	0.01	0.00
4.	0.01	0.00
5.	0.01	0.00
6.	0.01	0.00
7.	0.01	0.00
8.	0.01	0.00
9.	0.01	0.00
10.	0.02	0.01
11.	0.02	0.01
12.	0.03	0.00
13.	0.01	0.01
14.	0.02	0.01
15.	0.03	0.01
16.	0.01	0.01
17.	0.02	0.01
18.	0.03	0.01

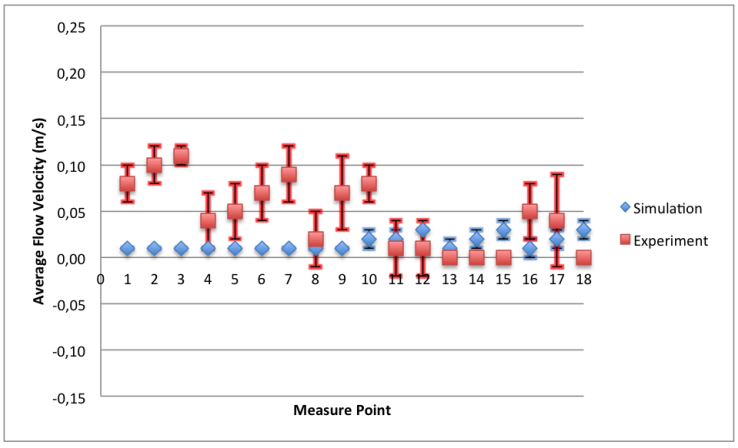

Figure 42: Simulation vs. Experiment for Location E, Pump Level 6.

The curve for the experiment seen in figure 41 is relatively consistent with the curve in figure 42. Measure points 1 to 7 do all have values within the expected range, while measure point 8 stand out. Measure point 8 is in the upper right centre (see setup 2 in table 14), and

have quite different averages than the measure point above or below. This is likely caused by a swirl or secondary current that may change the direction of the flow. Measure point 8 and all the other measure points in the proximity of 8 have relatively large SDs. The large SDs indicate fluctuations in the current which might contribute to the low flow velocity in measure point 8.

All the remaining measure points follow the expected curve.

The simulation indicates hardly any flow in the whole measuring region, albeit some fluctuations at the deeper measuring points (from 10 to 18).

6 Conclusion

The measure points were placed on each side of the centre of the turbine, but with a distance apart that put the points on the edge of the turbine. To improve the quality of the measurements the center for the measure points should go through the centre of the turbine wheel, and a shorter distance between the horizontally aligned points to get more information behind the turbine.

The probability that the results from both simulation with pump level 3.5 and 6 are mesh dependent is big. The downsizing of the mesh that was necessary to run the CFX-solver, the unfavourable Y^+ values, no time to perform mesh dependency tests and regulations, all speak towards mesh dependent results. This does not, however, carry the weight alone to state that the simulation results are wrong. But the reliability of the results should be questioned.

Instrument B performed satisfactory.

Due to the displaced flow trajectory from the real nozzle and the failure of the modelled nozzle to capture this, it is impossible to directly compare the two, and therefore impossible to make conclusions about the performance of the modelled nozzle.

Even though the experimental system and modelled system were not directly comparable, the results from the experiment with pump level 3.5 could not degrade the credibility of the constituent simulation, and neither could the CFD simulation degrade the experimental results. In both cases did most of the flow pass through the turbine. When discussing the results from the two, there were not found any questions that did not have a probable answer.

Since the experimental and modelled system cannot be compared directly, no conclusion can be drawn for whether the simulation with pump level 6 was wrong or not. However, that the turbine would drive the water current rather than being driven by the current is deemed unlikely. The simulation does give root to questions which have been found difficult to answer, and is for that reason estimated to be improbable.

The nozzles performance was judged upon its ability to have an evenly spread flow after it has passed through a pipe expansion from 100 mm to 300 mm in diameter, and a 90 degree bend. Table **??** and **??** documents the spread of the flow, and for the purpose of this experiment the nozzle performed satisfactory.

It was found for both pump level 3.5 and 6 that the nozzle was tilted backwards. The water flow exiting the nozzle had also a trajectory a little towards the right of the center of the turbine. The backward tilt of the nozzle could have been prevented by relatively easy means, and the blame for the tilt will therefore not be pinned on the nozzle. It is unclear if the horizontal displacement of the flow was solely caused by the twists in the inner pipes of the nozzle, or if there were also an angular displacement of the nozzle. If the twist in the inner pipes was the cause of the flow displacement, then that would be a constructional

failure that can be rectified.

It was indicated in the experimental results for pump level 6 that most of the flow entered the turbine, but with a larger portion going under the turbine than seen for pump level 3.5. The results also indicated that the water flow had a trajectory upward and to the right, just like what was observed for pump level 3.5. The experimental results for pump level 6 do have trend similarities with the other experiment, and the differences may be caused by the increased water flow.

References

ANSYS Inc. *Introduction to ANSYS Mesh*. Canonsburg, PA - USA, October 2012a.

ANSYS Inc. *Introduction to ANSYS CFX*. Canonsburg, PA - USA, October 2012b.

ANSYS Inc. *Introduction to ANSYS DesignModeler*. ANSYS Inc, Canonsburg, PA - USA, 2012c.

Allience for Rural Electrification. Renewable energy technologies for rural areas, n.d. URL `http://www.ruralelec.org/8.0.html?&L=%5C%5C%5C%5C%5C%5C%5C%22%3E%3Ca%20href%3D`.

Richard Furness. Experimental and theoretical studies in large diameter water pipes, 2007. URL `http://www.jdfandassociates.com/Technical/Large%20pipe%20flow.pdf`.

W. Malalasekera H. K. Versteeg. *An Introduction to Computational Fluid Dynamics, The Finite Volume Method*. Longman Scientific and Technical, 1995.

Martin Holst. Ansys. Phone Conference, 2014.

International Energy Agency (IEA. Energy poverty, n.d. URL `http://www.iea.org/topics/energypoverty/`.

et al. J. A. C. Orme. Investigation of the effect of biofouling on the efficiency of marine current turbines. Technical report, University of Wales Swansea, UK, 2001.

et al. J. F. Douglas. *Fluid Mechanics, 5th Edition*. Pearson Education Limited, 2005.

J. E. Quaicoe M.J. Khan, M.T. Iqbal. River current energy conversion systems: Progress, prospects and challenges. pages 2177–2193, 2008. doi: 10.1016/j.rser.2007.04.016.

NORWEA. Eksport kontrakt på fornybar energi!, 12 2013. URL `http://www.norwea.no/Files/Filer/Nyhetsbrev%20fra%20andre/Pressemelding_Deep%20River.pdf`.

et al. S. Szabó. Energy solutions in rural africa: mapping electrification costs of distributed solar and diesel generation versus grid extension. 6(3), 2011. doi: 10.1088/1748-9326/6/3/034002.

Guido Glania Simon Rolland. Hybrid mini-grids for rural electrification: Lessons learned, March 2011.

Kari Sørnes. Small-scale water current turbines for river applications, 2010.

Reidar Vestby. Deep river as, 2014.

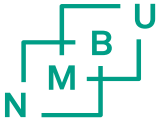

Norwegian University
of Life Sciences

Postboks 5003
NO-1432 Ås, Norway
+47 67 23 00 00
www.nmbu.no